NASA Technical Memorandum 86301 NASA-TM-86301 19840025453

ANALYSIS OF INSTABILITY-RELATED GROWTH OF A THROUGH-WIDTH DELAMINATION

JOHN D. WHITCOMB

SEPTEMBER 1984

National Aeronautics and
Space Administration

Langley Research Center
Hampton, Virginia 23665

SUMMARY

When a laminated composite is subjected to compressive loads, a delaminated region may buckle. This causes high interlaminar stresses at the delamination front and the delamination may grow. The effect of various parameters on instability-related delamination growth was studied analytically. The configuration studied consisted of a thick composite laminate with a single through-width delamination located near one surface. Both mechanical and thermal loads were considered. All conclusions were based on the assumption that G_I and G_{II} govern delamination growth. An approximate superposition stress analysis was developed which gives closed form expressions for G_I and G_{II}. The simplicity of the analysis permitted examination of numerous configurations. Both G_I and G_{II} were found to be very sensitive to delamination length and location through the thickness. The magnitude of G_I was also very sensitive to initial imperfection. Critical loads for delamination growth were calculated based on three growth criteria. Large differences in the predictions highlight the need for a verified mixed-mode delamination growth criterion.

INTRODUCTION

In laminated composites under compression loads, a delaminated region may buckle. When this happens, high interlaminar stresses can exist at the delamination front and the delamination may grow. Such delamination growth is referred to herein as "instability-related delamination growth" or IRDG. The mechanism of IRDG has been observed in a variety of specimens. Under compression fatigue, specimens with circular holes develop delaminations near the holes. These delaminated regions buckle, which causes IRDG (ref. 1). Delaminations in impacted specimens also have been observed to buckle and grow (refs. 2-6). In several studies, specimens with single delaminations have been made by imbedding Teflon or Kapton film in the laminate during manufacture (refs. 3, 7-13). When tested in compression, the specimens exhibited delamination growth caused by local buckling of the delaminated plies.

The prediction of instability-related delamination growth is complicated by the highly nonlinear character of the deformation. At the heart of the IRDG mechanism is a postbuckling process. The postbuckling behavior of a column or plate is very sensitive to the in-plane dimensions, the flexural and in-plane stiffnesses, and the initial imperfections. Hence, the growth of a delamination due to local buckling is expected to be sensitive to these same parameters. Other parameters expected to affect IRDG are the type of loading (i.e., mechanical or thermal), and, of course, the interlaminar fracture toughness.

The configuration studied (fig. 1) consists of a thick composite laminate with a single delamination located near one surface. The delamination is rectangular and extends across the entire specimen width. This configuration is perhaps the simplest that exhibits IRDG. Even so, the response to mechanical and thermal loads is still very complicated. Reference 14 presents a closed

form analysis of this configuration which calculates total strain-energy release rate. But studies (e.g., refs. 10, 15) have shown that the mode I fracture toughness is much lower than the mode II fracture toughness. Hence, an analysis is needed to calculate the components of strain energy release rate (G_I and G_{II}). References 7 and 8 used geometrically nonlinear finite element analyses to calculate G_I and G_{II} for several configurations. But the insight provided by strictly numerical analyses is very limited, since the results apply only to the particular configuration analyzed. Reference 8 dissected the original nonlinear configuration into linear configurations with nonlinearly related boundary conditions. The boundary conditions for this approximate superposition analysis are calculated using a simple strength of materials analysis. The relative simplicity of the resulting equations permits general conclusions to be made. For example, the equations show clearly the dependence of G_I and G_{II} on delamination length. Hence, results for one delamination length could be used immediately to calculate G_I and G_{II} for other delamination lengths.

The superposition analysis requires several constants which are calculated with a linear finite element analysis. In reference 8 these constants were independent of delamination length, applied load, and initial imperfection. A normalization technique developed in this study make the required constants independent of the flexural and axial stiffness of the buckled region. The original superposition analysis accounted for mechanical loads, whereas the new version also includes thermal loads.

The objectives of this paper are to describe the enhanced superposition analysis and to use this analysis to predict the effect of various parameters on instablity-related delamination growth. All conclusions are based on the assumption that G_I and G_{II} govern delamination growth.

NOMENCLATURE

a half-length of delamination before loading, m

Δa virtual crack closure distance used in strain-energy release rate, calculations, m

b specimen width, m

D bending stiffness of the buckled region given by

$$D = \frac{b}{3} \sum_{k=1}^{\rho} E^k \left[\left(\ell_k - \frac{t_c}{2} \right)^3 - \left(\ell_{k-1} - \frac{t_c}{2} \right)^3 \right], \ Nm^2$$

where ρ = number of plies

d_{x1}, d_{y1} unit load solutions for displacements near crack tip for load case $(P_C - P_D)$, m/N

d_{x2}, d_{y2} unit load solutions for displacements near crack tip for load case M, N^{-1}

$\bar{d}_{x1}, \bar{d}_{y1}$ normalized values of d_{x1} and d_{y1}, $mN^{-1/2}$

$\bar{d}_{x2}, \bar{d}_{y2}$ normalized values of d_{x2} and d_{y2}, $mN^{-1/2}$

E^k Young's modulus for ply k, MPa

E_{11}, E_{22}, E_{33} Young's moduli of unidirectional ply. The subscripts 1, 2, and 3 refer to the longitudinal, transverse, and thickness directions, respectively, MPa

F_{x1}, F_{y1} unit load solutions for forces at crack tip for load case $(P_C - P_D)$

F_{x2}, F_{y2} unit load solutions for forces at crack tip for load case M, m^{-1}

$\bar{F}_{x1}, \bar{F}_{y1}$ normalized values of F_{x1}, F_{y1}, $N^{1/2}$

$\bar{F}_{x2}, \bar{F}_{y2}$ normalized valules of F_{x2}, F_{y2}, $N^{1/2}$

G_I mode I strain-energy release rate, J/m^2

G_{II} mode II strain-energy release rate, J/m^2

G_{12}, G_{13}, G_{23} shear moduli for unidirectional ply, MPa

G_M strain-energy release rate related to moment at crack tip, J/m^2

G_T total strain-energy release rate, J/m^2

ℓ_{k-1} distance from top surface of laminate to ply "k"; top ply is ply 1, m

M moment, Nm

P_A, P_B, P_C, P_D axial loads carried in regions A, B, C, and D, respectively, N

P_T remote applied compressive load, N

P_{TM}^c mechanical load for bifurcation buckling when there is no thermal load, N

S_A, S_B, S_C, S_D axial stiffness of regions A, B, C, and D given by

$$S = b \sum_{k=1}^{\rho} E^k (\ell_k - \ell_{k-1})$$

where ρ = number of plies, N

ΔT increase in temperature, °K

t_B, t_C thickness of regions B and C, respectively, m

x, y rectangular Cartesian coordinates, m

α_A, α_D axial coefficients of thermal contraction for regions A and D, respectively, $°K^{-1}$

β thermal load, N

δ lateral deflection at $x = -a$ due to applied load, m

δ_o lateral deflection at $x = -a$ before application of mechanical or thermal load, m

ε axial strain; compressive strain is defined to be positive

ANALYSIS

Two analyses were used in this study: geometrically nonlinear, two-dimensional finite element analysis and an approximate superposition analysis. A geometrically nonlinear finite element analysis was used to illustrate the sensitivity of G_I and G_{II} to various geometric and material parameters. It was also used as a check for a simpler, but less rigorous, superposition analysis. Details of the geometrically nonlinear analysis are given in reference 7. The finite element models were similar to those described in reference 8.

The second analysis used was an approximate superposition analysis. This analysis is an extension of that presented in reference 8. In the following subsections, the approximate superposition analysis will be discussed first. Then the procedure for calculating G_I and G_{II} is described. Then the normalized constants for the superposition analysis are derived. Normalized strain-energy release rate curves for G_I and G_{II} versus applied load are described for the case of no initial imperfection. Finally, the material properties are discussed.

Approximate Superposition Analysis

Superposition techniques have been widely used in linear stress analysis to represent a complicated problem as a combination of several simpler problems. Application of the principle of superposition to nonlinear problems first requires a transformation that results in a linear system.

The key to the transformation is replacement of the source of nonlinearity with equivalent loads (figs. 2(a) and (b)). Because of symmetry only half of the configuration is considered. The buckled region (which responds nonlinearly due to significant rotations) is replaced by the loads P_D and M, the axial load and moment, respectively, in the column where it is cut (fig. 2(b)). The governing equations for the new configuration are linear. There are four nonlinearly related loads: three mechanical loads P_T, P_D, and M, and internal loads due to the thermal initial strain. Figure 2(b) shows the mechanical load P_T replaced by P_B and P_C, the portion of the applied load carried by regions B and C, respectively. The magnitudes of P_B and P_C are determined by solving equations (1a) through (1c).

$$P_B + P_C = P_T \tag{1a}$$

$$P_B = S_A(\varepsilon - \alpha_A \Delta T) \tag{1b}$$

$$P_C = S_D(\varepsilon - \alpha_D \Delta T) \tag{1c}$$

Equations (1) are based on the assumption that the axial strain ε is constant through the thickness of regions B and C. This assumption is valid if there is negligible bending in regions B and C.

The load system in figure 2(c) (which is the same as in fig. 2(b)) can be divided into the two load systems shown in figures 2(d) and 2(e). Because P_C and P_B are calculated using rule of mixtures (including thermal effects), the load system in figure 2(e) causes a uniform axial strain state and no interlaminar stresses. Consequently, to calculate interlaminar stresses, only the load system in figure 2(d) (i.e., $(P_C - P_D)$ and M) need be considered. Accordingly, in the current study involving strain-energy release rates, the configuration in figure 2(d) is the linearized equivalent of the nonlinear problem in figure 2(a). Note that the configuration in figure 2(d) has no initial strains due to thermal loads; all relevant thermal effects are included in P_C.

Appendix A describes a strength of materials analysis for calculating P_C, P_D, and M. The key equations from the appendix are

$$P_T = \frac{\pi^2 S_A}{a^2} \frac{(\delta^2 + 2\delta\delta_o)}{16} + \frac{D(S_A + S_D)}{S_A S_D} \frac{\delta}{\delta + \delta_o} - (\alpha_A - \alpha_D) \Delta T S_A \tag{2}$$

$$P_C = \frac{S_D}{S_A + S_D}[P_T + S_A \Delta T(\alpha_A - \alpha_D)] \tag{3}$$

$$P_D = \frac{\pi^2 D}{a^2} \frac{\delta}{\delta + \delta_o} \tag{4}$$

$$M = \frac{\pi^2 D \delta}{2a^2} \tag{5}$$

Equations (2) through (4) can be combined to obtain an expression for $P_C - P_D$

$$P_C - P_D = \frac{\pi^2}{16a^2} \frac{S_A S_D}{S_A + S_D} (\delta^2 + 2\delta\delta_o) \tag{6}$$

To use the loads $(P_C - P_D)$ and M in a two-dimensional analysis requires that they be expressed as an equivalent distribution of tractions. To calculate this distribution, the axial strains were assumed to vary linearly through the thickness where the tractions are applied (i.e., at the cut). Intuitively, this seems to be reasonable if region D (fig. 2) is not cut too close to the crack tip. The validity of the assumed linear variation was established in reference 8.

Linear finite element analysis was used to calculate the response of the linearized configuration in figure 2(d) to unit values of $(P_C - P_D)$ and M. Because the configuration is linear, the solution for any arbitrary combination of $(P_C - P_D)$ and M is simply a linear combination of the unit load responses. If region B (fig. 2) is much thicker than region C, the unit load solutions are very insensitive to delamination length. In the current study the ratio of thicknesses, t_B/t_C, was always large (i.e., at least 9/1). As demonstrated in a later section, the unit load solutions can be normalized in such a way that the normalized parameters become independent of the in-plane and flexural stiffness of the buckled region.

Delamination length, initial imperfection, applied load, and temperature changes are all accounted for in the strength of materials analysis in calculating $(P_C - P_D)$ and M.

Strain-Energy Release Rate

The virtual crack closure method (ref. 16) was used to calculate mode I and mode II strain-energy release rates, G_I and G_{II}, respectively. The forces transmitted through the node at the crack tip and the relative displacements of the two nodes on the crack boundary closest to the crack tip were used in the calculation. Equations (7) show how this technique is used for the superposition stress analysis.

$$G_I = \frac{1}{2\Delta ab}\left[(P_C - P_D)F_{y1} + MF_{y2}\right]\left[(P_C - P_D)d_{y1} + Md_{y2}\right]$$

$$G_{II} = \frac{1}{2\Delta ab}\left[(P_C - P_D)F_{x1} + MF_{x2}\right]\left[(P_C - P_D)d_{x1} + Md_{x2}\right] \tag{7}$$

In these equations F_x, F_y, d_x, and d_y are the unit load values of the nodal forces and the corresponding relative nodal displacements in the x- and y-directions. (The coordinate system is defined in fig. 2.) The superscripts 1 and 2 on the unit load parameters identify parameters associated with $(P_C - P_D)$ and M, respectively.

If the distance is small between the crack tip and the nodes used to calculate relative displacements (which it should be for accurate results), then $F_{y1}/d_{y1} = F_{y2}/d_{y2}$ and $F_{x1}/d_{x1} = F_{x2}/d_{x2}$. Using these relationships in equations (7) results in

$$G_I = \frac{1}{2\Delta ab}\frac{d_{y1}}{F_{y1}}\left[(P_C - P_D)F_{y1} + MF_{y2}\right]^2$$

$$G_{II} = \frac{1}{2\Delta ab}\frac{d_{x1}}{F_{x1}}\left[(P_C - P_D)F_{x1} + MF_{x2}\right]^2 \tag{8}$$

Reference 8 gives the unit load solutions for one laminate. The next section describes a normalization procedure which allows use of these same values for many different laminates.

Normalized Unit Load Solutions

The effect of the buckled region's in-plane and flexural stiffness on the unit load solutions can be approximated using strength of materials analysis. This approximation depends on the following two assumptions:

1. The crack tip compliances $(d_{xl}/F_{xl}$, d_{yl}/F_{yl}, etc.) do not vary with the in-plane and flexural stiffnesses of the buckled region. Hence, the material properties immediately around the crack tip should not be changed.
2. The ratios G_I/G_{II} for $(P_C - P_D)$ and M applied individually are independent of the in-plane and flexural stiffnesses of the buckled region.

Implicit in these assumptions is that region A is much thicker than region D. The accuracy of these assumptions will be evaluated later. The required normalization is different for the two load cases $(P_C - P_D)$ and M, so each load case will be examined individually.

Load case 1: $(P_C - P_D)$

Using simple strength of materials analysis (see ref. 17) one can show that the total strain-energy release rate for the load case $(P_C - P_D)$ is

$$G_T = \frac{(P_C - P_D)^2}{2b} \frac{S_A + S_D}{S_A S_D} \tag{9}$$

From equations (8), the total strain-energy release rate is

$$G_T = G_I + G_{II} = \frac{1}{2\Delta ab}\left(P_C - P_D\right)^2\left[\frac{d_{y1}}{F_{y1}}\left(F_{y1}\right)^2 + \frac{d_{x1}}{F_{x1}}\left(F_{x1}\right)^2\right] \tag{10}$$

Combining equations (9) and (10) yields

$$\frac{1}{2\Delta ab}\left[\frac{d_{y1}}{F_{y1}}\left(F_{y1}\right)^2 + \frac{d_{x1}}{F_{x1}}\left(F_{x1}\right)^2\right] = \frac{S_A + S_D}{S_A S_D} \tag{11}$$

From assumption (1), the compliances d_{y1}/F_{y1} and d_{x1}/F_{x1} are constant. Since these compliances are constant, assumption (2) requires that F_{y1} and F_{x1} change by the same scale factor as S_A and S_D are changed. Hence, the normalized unit load solutions $\bar{F}_{y1}$ and $\bar{F}_{x1}$, which are independent of S_A and S_D, are

$$\bar{F}_{y1} = F_{y1}\left(\frac{S_A S_A}{S_A + S_D}\right)^{1/2} \quad \text{and} \quad \bar{F}_{x1} = F_{x1}\left(\frac{S_A S_D}{S_A + S_D}\right)^{1/2} \tag{12}$$

Since the crack-tip compliances d_{x1}/F_{x1} and d_{y1}/F_{y1} are assumed to be constant, the normalized unit load displacements are

$$\bar{d}_{x1} = d_{x1}\left(\frac{S_A S_D}{S_A + S_D}\right)^{1/2} \quad \text{and} \quad \bar{d}_{y1} = d_{y1}\left(\frac{S_A S_D}{S_A + S_D}\right)^{1/2} \tag{13}$$

Therefore, if the unit load solutions are known for one combination of S_A and S_D, the normalized unit load forces and displacements can be calculated using equations (12) and (13). Then these normalized parameters can be used with equations (14) to calculate the unit load solutions for other combinations of S_A and S_D.

$$F_{x1} = \bar{F}_{x1}\left(\frac{S_A + S_D}{S_A S_D}\right)^{1/2}$$

$$d_{x1} = \bar{d}_{x1}\left(\frac{S_A + S_D}{S_A S_D}\right)^{1/2}$$

$$F_{y1} = \bar{F}_{y1}\left(\frac{S_A + S_D}{S_A S_D}\right)^{1/2} \qquad (14)$$

$$d_{y1} = \bar{d}_{y1}\left(\frac{S_A + S_D}{S_A S_D}\right)^{1/2}$$

Load case 2: M

Again, simple strength of materials arguments are used to derive an expression for the total strain-energy release rate (eq. (15))

$$G_T = \frac{M^2}{2Db} \qquad (15)$$

Following the same procedures used for load case 1, the normalized unit load solutions are found to be

$$\bar{F}_{x2} = F_{x2} D^{1/2} \qquad \bar{d}_{x2} = d_{x2} D^{1/2}$$

$$\bar{F}_{y2} = F_{y2} D^{1/2} \qquad \bar{d}_{y2} = d_{y2} D^{1/2} \qquad (16)$$

After the unit load solutions are calculated for one value of D, the normalized unit load solutions can be calculated using equations (16). These

normalized solutions can be used with equations (17) to calculate the unit load solutions for other values of D.

$$F_{x2} = \bar{F}_{x2} D^{-1/2}$$

$$d_{x2} = \bar{d}_{x2} D^{-1/2}$$

$$F_{y2} = \bar{F}_{y2} D^{-1/2} \qquad (17)$$

$$d_{y2} = \bar{d}_{y2} D^{-1/2}$$

Therefore, the mode I and mode II strain-energy release rates for a range of S_A, S_D, and D can be calculated by combining equations (8), (14), and (17).

$$G_I = \frac{1}{2\Delta ab} \frac{d_{y1}}{F_{y1}} \left[(P_C - P_D) \bar{F}_{y1} \left(\frac{S_A + S_D}{S_A S_D} \right)^{1/2} + M\bar{F}_{y2} D^{1/2} \right]^2$$

(18)

$$G_{II} = \frac{1}{2\Delta ab} \frac{d_{x1}}{F_{x1}} \left[(P_C - P_D) \bar{F}_{x1} \left(\frac{S_A + S_D}{S_A S_D} \right)^{1/2} + M\bar{F}_{x2} D^{1/2} \right]^2$$

The accuracy of these derived unit load solutions depends on how much different the current configuration is from the configuration which was analyzed with the finite element analysis. Obviously, one should use the finite element analysis on the configuration which lies in the middle of the range of interest. The unit load solutions for the laminates considered herein are given in Table 1.

Note that equations (9) and (15) can be summed to obtain a very simple expression for the total strain-energy release rate, G_T for combined loading (i.e. $(P_C - P_D)$ and M).

$$G_T = \frac{(P_C - P_D)^2}{2b} \frac{S_A + S_D}{S_A S_D} + \frac{M^2}{2Db} \tag{19}$$

This simple summation is possible because there is no coupling between $(P_C - P_D)$ and M in terms of the potential energy of the applied loads.

Normalized Strain-Energy Release Rate Curves for the Case $\delta_o = 0$

In the preceding sections equations are presented which allow calculation of G_I and G_{II}. These equations are easily solved for any applied load (mechanical or thermal or both). Additional insight is possible if parameters are identified which coalesce the G_I and G_{II} vs. applied load curves for various configurations into a single curve. Reference 8 showed that by plotting a^2P_T vs. a^4G_I, the G_I vs. P_T curves for various delamination lengths coalesce into a single curve. In the current study parameters were derived which provide a single curve for arbitrary length and in-plane and flexural stiffnesses of the buckled region. Also, the loading can be mechanical, thermal, or combined mechanical and thermal. The curve derived herein is only valid when the initial imperfection δ_o is zero.

The key to deriving the normalized curves is expressing P_T, $(P_C - P_D)$, and M in terms of the normalized load parameter $\bar{P}_T$ (eq. (20)):

$$\bar{P}_T = \frac{P_T + \beta}{P_{TM}^c} - 1 \tag{20}$$

where $\beta = (\alpha_A - \alpha_D)\,\Delta T S_A$ = thermal load

P_T = mechanical load

P_{TM}^c = mechanical load for buckling for case in which $\beta = 0$

The parameter P_{TM}^c is determined from equation (1) by substituting $\delta = \delta_o = \Delta T = 0$. The result is

$$P_{TM}^{c} = \frac{\pi^2 D}{a^2} \frac{S_A + S_D}{S_D} \tag{21}$$

Combining equations (2), (20), and (21) yields an expression relating normalized load to lateral deflection.

$$\bar{P}_T = \frac{S_A S_D}{16D(S_A + S_D)} \delta^2 \tag{22}$$

Equations (3), (4), (21), and (22) can be combined to yield an expression for $(P_C - P_D)$ in terms of $\bar{P}_T$.

$$(P_C - P_D) = \frac{\pi^2 D}{a^2} \bar{P}_T \tag{23}$$

Equations (5) and (22) can be combined to yield an expression for M in terms of $\bar{P}_T$.

$$M = \frac{2\pi^2 D}{a^2} \left[\frac{D(S_A + S_D)}{S_A S_D}\right]^{1/2} \bar{P}_T^{1/2} \tag{24}$$

If the expressions for $(P_c - P_D)$ and M in equations (23) and (24) are combined with equation (18), we obtain equations for G_I and G_{II} in terms of $\bar{P}_T$.

$$G_I = \frac{1}{2\Delta ab} \frac{d_{y1}}{F_{y1}} \frac{\pi^4}{a^4} D^2 \frac{S_A + S_D}{S_A S_D} \left(\bar{P}_T \bar{F}_{y1} + 2\bar{P}_T^{1/2} \bar{F}_{y2} \right)^2$$

$$G_{II} = \frac{1}{2\Delta ab} \frac{d_{x1}}{F_{x1}} \frac{\pi^4}{a^4} D^2 \frac{S_A + S_D}{S_A S_D} \left(\bar{P}_T \bar{F}_{x1} + 2\bar{P}_T^{1/2} \bar{F}_{x2} \right)^2 \quad (25)$$

Next, both sides of equations (25) are divided by $\frac{D^2(S_A + S_D)}{a^4 S_A S_D}$ to obtain normalized strain-energy release rate parameters which are functions of $\bar{P}_T$ alone.

$$G_I \, a^4 \frac{S_A S_D}{D^2(S_A + S_D)} = \frac{\pi^4}{2\Delta ab} \frac{d_{y1}}{F_{y1}} \left(\bar{P}_T \bar{F}_{y1} + 2\bar{P}_T^{1/2} \bar{F}_{y2} \right)^2$$

$$G_{II} \, a^4 \frac{S_A S_D}{D^2(S_A + S_D)} = \frac{\pi^4}{2\Delta ab} \frac{d_{x1}}{F_{x1}} \left(\bar{P}_T \bar{F}_{x1} + 2\bar{P}_T^{1/2} \bar{F}_{x2} \right)^2 \quad (26)$$

Hence, the $G_I \frac{a^4 S_A S_D}{D^2(S_A + S_D)}$ or $G_{II} \frac{a^4 S_A S_D}{D^2(S_A + S_D)}$ vs. $\bar{P}_T$ curves for different configurations should all coincide. This will be verified in the Results and Discussion section.

Materials Properties

The unidirectional ply properties were assumed to be

$E_{11} = 140$ GPa

$E_{22} = E_{33} = 14$ GPa

$\nu_{12} = \nu_{13} = \nu_{23} = 0.21$

$$G_{12} = G_{13} = G_{23} = 5.9 \text{ GPa}$$

Plane strain (i.e., $\varepsilon_z = 0$) and $\varepsilon_{xz} = 0$ were imposed to calculate the 2D properties. In regions where coarse finite elements spanned several plies, laminate theory was used to obtain average properties. Lamina thickness was assumed to be 0.14 mm.

RESULTS AND DISCUSSION

A parametric study of instability-related delamination was performed. The parameters considered are delamination length, in-plane and flexural stiffness of the buckled region, initial imperfections, mechanical and thermal load, and interlaminar fracture toughness. Four laminate types are considered. These are described in Table 1. All conclusions are based on the assumption that G_I and G_{II} govern delamination growth.

First, G_I and G_{II} will be discussed for a variety of cases. When possible, simple expressions will be presented to quantify the effect of various parameters on G_I and G_{II}. When the effect of a parameter is not described by simple expressions, example results will be discussed which qualitatively illustrate the trends.

Next, the effect of various parameters on delamination growth is examined analytically. Several delamination growth criteria are considered. The assumed values of G_{Ic} and G_{IIc} range from values representative of brittle epoxy systems to tough thermoplastic systems.

Parametric Study of G_I and G_{II}

When the initial imperfection δ_o is zero, the equations for P_T, P_C, and P_D (eqs. (2), (3), and (4)) simplify considerably. The result is that simple equations for G_I and G_{II} (eqs. (26)) can be derived. These equations show clearly the effect of various parameters on the relationship

between G_I, G_{II}, and normalized load $\bar{P}_T$. When $\delta_o \neq 0$, the expressions for G_I and G_{II} are not so simple. Hence, in this section the cases $\delta_o = 0$ and $\delta_o \neq 0$ will be discussed separately. The case $\delta_o = 0$ will be discussed first.

When $\delta_o = 0$, equations (26) express the relationships between G_I, G_{II}, and normalized load $\bar{P}_T$ for arbitrary values of a, S_A, S_D, and D. For a given value of $\bar{P}_T$, the magnitudes of G_I and G_{II} vary as $\frac{D^2(S_A + S_D)}{a^4 S_A S_D}$. Hence, small changes in flexural stiffness D or delamination length 2a should result in large changes in G_I and G_{II}. Changes in S_A and S_D also should affect G_I and G_{II}. Figure 3 verifies this prediction. Figure 3(a) shows the effect of delamination length on G_I and G_{II} and figure 3(b) shows the effect of changing D, S_A, and S_D through variations in laminate type. These results were obtained with geometrically nonlinear finite element analysis. The results are plotted on semi-log scales -- hence, the differences between the curves represent very large differences. Figure 3 shows that G_I first increases, then decreases with increasing applied load. This peculiar behavior is explained in reference 7. Figure 4 shows that equations (26) accurately quantify the effects of D, a, S_A, and S_D on G_I and G_{II}. By plotting $a^4 \frac{S_A S_D}{D^2(S_A + S_D)} G_I$ vs. $\bar{P}_T$ and $a^4 \frac{S_A S_D}{D^2(S_A + S_D)} G_{II}$ vs. $\bar{P}_T$, all of the data in figures 3(a) and 3(b) have been reduced to one curve for G_I and one for G_{II}. The curves in figure 4 are plotted on linear scales. Hence, the scatter is quite small. Also, figure 4 shows that if nonlinear finite element results are available for one configuration, the G_I and G_{II} values for other configurations can be estimated immediately.

Equation (2) shows that the thermal load $\beta = (\alpha_A - \alpha_D)\Delta TS_A$ simply shifts the relationship between P_T and δ. This shift causes a shift in the G_I and G_{II} vs. P_T relationship. Figure 5(a) shows finite element results for two different thermal loads. The two curves have nearly the same shape, but they are offset by the magnitude of the thermal load. The normalized load $\bar{P}_T$ includes the effect of the thermal load, hence the two curves agree quite well when normalized G_I vs. $\bar{P}_T$ is plotted (fig. 5(b)). In figure 5(a), for one of the cases G_I is nonzero when $P_T = 0$. This simply means that the thermal load alone was sufficient to buckle the sublaminate. In fact, for large thermal loads, delamination growth may occur without any applied mechanical load.

As previously noted, when $\delta_o \neq 0$ the expressions for G_I and G_{II} are not nearly as simple as when $\delta_o = 0$. Consequently, the effect of δ_o on G_I and G_{II} is not obvious from the govening equations. Using figures 6 through 10 the effect of δ_o on G_I and G_{II} is qualitatively assessed by examining particular results of the approximate superposition analysis.

Herein, the term "initial imperfection" refers to the lateral distortion which would exist if the specimen was stress-free, i.e., without mechanical, thermal, or hygroscopic stresses. A possible cause of an initial imperfection is an inclusion left between lamina during fabrication.

Figure 6 shows the effect of δ_o on G_I and G_{II}. Because normalized strain-energy release rates are plotted vs. normalized load, the curves for different delamination lengths are the same. There are, however, different curves for different values of δ_o. Note that G_I is very sensitive to δ_o, whereas G_{II} is almost insensitive to δ_o. The peak value of G_I decreases rapidly as δ_o increases. In fact, if $\bar{P}_T$ is greater than about 0.2, G_I decreases with increased δ_o. When $\bar{P}_T$ is negative, the applied load is

insufficient to cause bifurcation buckling, i.e., buckling of a perfectly straight column. But when $\delta_o \neq 0$, lateral deflections occur as soon as compressive stresses develop in the delaminated region. Concomitantly, non-zero values of G_I and G_{II} occur for $-1 < \bar{P}_T < 0$. In this region G_I and G_{II} may increase with increased δ_o. Therefore, if a delamination is short and is located deep in the interior of a laminate and if $\delta_o = 0$, then the operating strain is unlikely to be sufficiently large to cause bifurcation buckling. Hence, G_I and G_{II} would be zero and delamination growth would not occur. But if $\delta_o \neq 0$, G_I and G_{II} can exist even for relatively small strain, and growth might occur.

Figure 7 shows the effect of δ_o on G_I and G_{II} for three laminates with different values of S_A, S_D, and D. In figure 7 the solid curve is for the case $\delta_o = 0$. The dashed curves are for the case $\delta_o = 0.1$ mm. As shown earlier, the curves for all three configurations are the same when $\delta_o = 0$. When $\delta_o \neq 0$ there is a different curve for each combination of S_A, S_D, and D. The effect on G_I is much larger than the effect on G_{II}. As the flexural stiffness of the buckled region increases the effect of δ_o on G_I decreases. (The flexural stiffness is largest for laminate type 4 and smallest for laminate type 1.)

Figure 8 shows the effect of δ_o on the G_I/G_{II} ratio. For all values of $\bar{P}_T$ the ratio G_I/G_{II} decreases as δ_o increases. For all values of δ_o the ratio G_I/G_{II} decreases rapidly as $\bar{P}_T$ increases. Therefore, whether delamination growth is governed by G_I or G_{II} is likely dependent on the magnitudes of δ_o and $\bar{P}_T$.

Earlier it was pointed out that thermal loads can cause buckling when the applied load P_T is zero. The lateral deflection due to thermal load may be visually indistinguishable from an initial imperfection δ_o. But the thermal

load β affects G_I and G_{II} differently than δ_o. Figure 9 illustrates the difference. For reference the case $\delta_o = 0$, $\beta = 0$ is also included. The magnitudes of δ_o and β were chosen such that when $P_T = 0$, the lateral distortion was the same for both cases. The thermal load case has a larger value of G_I than the initial imperfection case for all values of P_T. The value of G_{II} was also found to be larger for the thermal case. (This result is not included in fig. 9.) The lateral deflection increases more quickly for the thermal case than for the intial imperfection case.

Prediction of Delamination Growth

To predict the critical load for delamination growth (herein referred to as the "critical load") requires three types of information: (1) the relationship between applied load and strain-energy release rates, (2) the growth criterion $\left(\text{e.g., } \left(\frac{G_I}{G_{Ic}}\right)^2 + \left(\frac{G_{II}}{G_{IIc}}\right)^2 = 1\right)$, and (3) the material constants to be used in the growth criterion (e.g., G_{Ic} and G_{IIc}). The relationship between applied load and strain-energy release rates can be determined using the analysis described herein. At this time there is no widely accepted delamination growth criterion for mixed-mode configurations. Hence, several criteria will be considered. The three criteria selected are given in equations (27) through (29).

$$G_I = G_{Ic} \tag{27}$$

$$G_M = G_{Ic} \tag{28}$$

$$\left(\frac{G_I}{G_{Ic}}\right)^2 + \left(\frac{G_{II}}{G_{IIc}}\right)^2 = 1 \tag{29}$$

The criterion $G_I = G_{Ic}$ assumes that only the mode I component is important. The criterion $G_M = G_{Ic}$ also assumes that only the mode I component is important. The quantity G_M is the strain-energy release rate due to the moment M at the delamination front. This criterion was proposed in reference 12. The mixed-mode criterion, equation (29), attempts to account for both the mode I and mode II effects. The mixed-mode criterion will be emphasized in the following discussion.

The material constants in the growth criteria considered consist of only G_{Ic} and G_{IIc}. Numerous studies have reported values of G_{Ic} (e.g., refs. 10, 15, 18, 19). These G_{Ic} values range from about 200 J/m^2 to 1000 J/m^2. The mode II fracture toughness G_{IIc} is less well characterized, but is generally assumed to be several times as large as G_{Ic}. Herein, the ratio G_{IIc}/G_{Ic} ranges from 1 to 5. The critical load is determined from the growth criterion equation and the equations for strain-energy release rates (i.e., G_I, G_{II}, or G_M). The procedures for solving the equations are given in Appendix B.

Figure 10 shows the variation of critical load with delamination length predicted by the three criteria in equations (27) through (29). In figure 11 the initial imperfection $\delta_o = 0$. The assumed values of G_{Ic} and G_{IIc} were 200 J/m^2 and 1000 J/m^2, respectively. The laminate is type 2, which has a $[0_4]$ buckled sublaminate. For short delaminations, all three criteria initially predict a reduction and then an increase in critical load with

increase in delamination length 2a. But beyond about 22 mm, even the trends are very different for the three criteria. The criterion $G_I = G_{Ic}$ predicts no growth, regardless of the applied load, beyond about 23 mm. The criterion $G_M = G_{Ic}$ predicts an increasing but finite critical load. The mixed-mode criterion predicts an almost constant critical load after the initial growth. The mixed-mode criterion and the criterion $G_M = G_{Ic}$ both predict that if a short delamination grows, there will be substantial unstable growth before arrest. The differences in the predictions from the three criteria highlight the need for a verified growth criterion.

The bifurcation buckling curve is shown as a dashed line in figure 10. For short delaminations there is little difference between the buckling load and the critical load for delamination growth. From a practical standpoint, a short delamination must not be permitted to buckle -- if it buckles, one must assume it will grow.

Figure 11 shows results analogous to those in figure 10 except that $\delta_o = 0.1$ mm. For short delaminations (i.e., < 15-20 mm), the initial imperfection reduces the critical load from that shown in figure 10. For long delaminations the initial imperfection has little effect. The criterion $G_I = G_{Ic}$ and the mixed-mode criterion agree for short delaminations (see figs. 10 and 11). Hence, the G_I component must dominate in the mixed mode criterion for short delaminations. For longer delaminations the G_{II} component dominates. The bifurcation buckling curve from figure 10 is shown in figure 11 for reference. (Actually, bifurcation buckling does not occur when there is an initial imperfection.) For short delaminations the bifurcation buckling load is larger than the critical load for growth. Therefore, if $\delta_o \neq 0$ it is unconservative to use the buckling load as an upper bound on the allowable load.

To expedite the remaining discussion, only the mixed-mode criterion will be used in the remainder of this paper.

The curves in figures 10 and 11 depend on the particular specified values of G_{Ic} and G_{IIc}. Of interest is how much the critical load increases for increases in G_{Ic} and G_{IIc}. Figure 12 shows the critical load predicted by the mixed-mode growth criterion for three combinations of G_{Ic} and G_{IIc}. The initial imperfection δ_o is zero for the cases in figure 12. For short delaminations large improvements in G_{Ic} only moderately increase the critical load and G_{IIc} has no effect. For long delaminations, G_{Ic} has no effect but increases in G_{IIc} result in substantial increase in the critical load. Figure 14 shows predicted critical loads for the case $\delta_o = 0.1$ mm. Comparison of figures 12 and 13 shows that the initial imperfection only affects the predictions for short delaminations; for short delaminations the initial imperfection reduces the critical load.

Uncertainty about the depth of a delamination (i.e., the thickness of the buckled region) and the magnitude of the initial imperfection causes significant uncertainty about the load at which a delamination will grow. Suppose that the buckled region has either 3 or 4 zero degree plies (laminates types 1 and 2). Figures 14 and 15 show the predicted critical load (using the mixed-mode criterion) for each possibility. Figure 14 shows predictions for the case $\delta_o = 0$. For short delaminations the thicker buckled region has a higher critical load, but the trend is reversed for long delaminations. Figure 15 shows results analogous to those in Figure 14 except that $\delta_o = 0.1$ mm. Comparison of figures 14 and 15 shows that the initial imperfection affects only the short delamination predictions. In the short delamination region the thicker laminate is affected more than the thinner one. In fact, for

δ_o = 0.1 mm the predicted critical loads are nearly the same for the two laminates in the short delamination region.

The results presented here should be helpful in designing specimens to test various delamination growth criteria. The sensitivity of G_I and G_{II} to various parameters illustrated in the figures indicates the accuracy with which these parameters must be known to obtain accurate values of G_I and G_{II}.

CONCLUSIONS

A parametric analytical study of instability-related delamination growth was conducted. All conclusions were based on the assumption that the mode I and mode II strain-energy release rates (G_I and G_{II}, respectively) govern delamination growth. The configuration studied consisted of a thick composite laminate with a single delamination located near one surface.

The primary accomplishments and conclusions from this study are:

1. An approximate superposition analysis was developed which gives closed form expressions for G_I and G_{II} for a wide range of delamination length and location through the thickness, initial imperfection, and mechanical and thermal load.

2. The magnitude of G_I is very sensitive to delamination length, initial imperfection, and delamination depth. For zero initial imperfection, simple expressions were derived which quantify the sensitivity to delamination length and delamination depth.

3. The ratio G_I/G_{II} decreases monotonically with applied load and initial imperfection.

4. Initial deflection due to residual thermal stresses is worse than initial deflection due to initial imperfection.

5. Three growth criteria were considered. The large differences in the predicted critical loads highlights the need for a verified mixed-mode growth criterion.

6. Short delaminations can be expected to grow if buckling occurs. This growth is likely to be rapid and extensive.

7. Initial imperfection can cause a design based on "no bifurcation buckling" to be very unconservative.

8. Based on the mixed-mode criterion:

(a) A large increase in G_{Ic} results in a moderate increase in critical load for delamination growth for short delaminations.

(b) A large increase in G_{IIc} results in a substantial increase in critical load for delamination growth for long delaminations.

REFERENCES

1. Phillips, E. P.: Effects of Truncation of a Predominantly Compression Load Spectrum on the Life of a Notched Graphite/Epoxy Laminate. Fatigue of Fibrous Composite Materials, ASTM STP 723, American Society for Testing and Materials, 1981, pp. 197-212.

2. Starnes, J. H., Jr.; Rhodes, Marvin D.; and Williams, Jerry G.: The Effect of Impact Damage and Circular Holes on the Compressive Stength of a Graphite-Epoxy Laminate. NASA TM 78796, Oct. 1978.

3. Byers, B. A.: Behavior of Damaged Graphite/Epoxy Laminates Under Compression Loading. NASA CR 159293, August 1980.

4. Rosenfeld, M. S.; and Gause, L. W.: Compression Fatigue Behavior of Graphite/Epoxy in the Presence of Stress Raisers. Fatigure of Fibrous Composite Materials, ASTM STP 723, American Society for Testing and Materials, 1981, pp. 174-196.

5. Starnes, J. H., Jr.; and Williams, J. G.: Failure Characteristics of Graphite/Epoxy Structural Components Loaded in Compression. NASA TM 84552, Sept. 1982.

6. Chai, H.; Knauss, W. G.; and Babcock, C. D.: Observation of Damage Growth in Compressively Loaded Laminates. Experimental Mechanics, vol. 23, Sept. 1983, pp. 329-337.

7. Whitcomb, J. D.: Finite Element Analysis of Instability-Related Delamination Growth. Journal of Composite Materials, vol. 15, Sept. 1981, pp. 403-426.

8. Whitcomb, J. D.: Strain Energy Release Rate Analysis of Cyclic Delamination Growth in Compressively Loaded Laminates. Effects of Defects in Composite Materials, ASTM STP 836, American Society for Testing and Materials, 1984, pp. 175-193.

9. Ramkumar, R. L.: Fatigue Degradation in Compressively Loaded Composite Laminates. NASA CR 165681, April 1981.

10. Ramkumar, R. L.: Performance of a Quantitative Study of Instability-Related Delamination Growth. NASA CR 166046, March 1983.

11. Gillespie, J. W.; and Pipes, R. B.: Compressive Strength of Composite Laminates with Interlaminar Defects. Composite Structures, vol. 2, no. 1, 1984, pp. 49-69.

12. Ashizaiwa, M.: Fast Interlaminar Fracture of a Compressively Loaded Composite Containing a Defect. Presented at the Fifth DOD/NASA Conference on Fibrous Composites in Structural Design, New Orleans, LA, Jan. 1981. (Available as Douglas Paper No. 6994.)

13. Konishi, D. Y.; and Johnston, W. R.: Fatigue Effects on Delaminations and Strength Degradation in Graphite/Epoxy Laminates. Composite Materials: Testing and Design (Fifth Conference), ASTM STP 674, S. W. Tsai, Ed., American Society for Testing and Materials, 1979, pp. 597-619.

14. Chai, H.; Babcock, C. D.; and Knauss, W. G.: One Dimensional Modeling of Failure in Laminated Plates by Delamination Buckling. Int. J. Solids and Structures, vol. 17, no. 11, 1981, pp. 1069-1083.

15. Wilkins, D. J.: A Comparison of the Delamination and Environmental Resistance of a Graphite/Epoxy and a Graphite-Bismaleimide. Naval Air Systems Command Report, NAV-GD-0037, 1981.

16. Rybicki, E. F.; and Kanninen, M. F.: A Finite Element Calculation of Stress Intensity Factors by a Modified Crack Closure Integral. Engineering Fracture Mechanics, vol. 9, no. 4, 1977, pp. 931-938.

17. Roderick, G. L.; Everett, R. A., Jr.; and Crews, J. H., Jr.: Cyclic Debonding of Unidirectional Composite Bonded to Aluminum Sheet for Constant Amplitude Loading. NASA TN D-8126, 1976.

18. O'Brien, T. K.; Johnston, N. J.; Morris, D. H.; and Simonds, R. A.: Determination of Interlaminar Fracture Toughness and Fracture Mode Dependence of Composites Using the Edge Delamination Test. Proceedings of the International Conference on Testing, Evaluation, and Quality Control of Composites, University of Surrey, Guilford, England, Sept. 1983, pp. 223-232.

19. Carlisle, D. R.; and Leach, D. C.: Damage and Notch Sensitivity of Graphite/Peek Composite. Proceedings of the 15th National SAMPE Technical Conference, Oct. 1983, pp. 82-93.

20. Brush, D. O.; and Almroth, B. L.: Buckling of Bars, Plates, and Shells. McGraw-Hill Book Co., Inc., New York, NY, 1975, pp. 13-14.

APPENDIX A

STRENGTH OF MATERIALS ANALYSIS

A strength of materials analysis is described herein for the configuration in figure 1.

The configuration is divided into four regions, as shown in figure 2. Because of symmetry, only half of the laminate is modeled. The laminate has width b. The following assumptions are made:

1. Regions B and C are perfectly bonded. Regions A and D are unbonded.
2. Regions A, B, and C have constant axial strain. Hence, the force-strain relations are those for a simple rod subjected to axial load and a temperature change; e.g.,

$$P_A = S_A(\varepsilon - \alpha_A \Delta T) \tag{A1}$$

   Since regions A, B, and C are not permitted to bend, global bending effects cannot be predicted by this idealization.
3. Region D has zero slope at both ends.
4. Region D is symmetric with respect to its midplane.
5. Regions A and B have a thermal contraction coefficient α_A.
6. Regions C and D have a thermal contraction coefficient α_D.
7. All regions experience the same ΔT.
8. Region D has an initial sinusoidal imperfection of peak magnitude δ_o. The term "initial imperfection" refers to the lateral distortion which would exist if the specimen was stress-free, i.e., without mechanical, thermal, or hygroscopic stresses. The initial shape is given by

$$v(x)\big|_{initial} = \frac{\delta_o}{2}\left(1 - \cos\frac{\pi x}{a}\right) \tag{A2}$$

where $v(x)$ = the distortion in the y-direction.

To describe the nonlinear behavior of region D, equations (A3) and (A4) for post-buckling of a column were used.

$$P_D = \frac{\pi^2 D}{a^2}\frac{\delta}{\delta + \delta_o} \qquad \text{(ref. 20)} \tag{A3}$$

$$a - \bar{a} = \frac{\pi^2}{16a}\left(\delta^2 + 2\delta\delta_o\right) + \frac{aP_D}{S_D} + a\alpha_D\Delta T \tag{A4}$$

where δ, a, $\bar{a}$, and P_D are peak lateral deflection, axial length before and after deformation, and load, respectively. Compression strain is defined to be positive. The derivation of equation (A4) for mechanical loads only can be formed in reference 12. The additional term for thermal loads, $a\alpha_D\Delta T$, requires no derivation. Equations (A3) and (A4) were derived using strength of materials analysis of a column.

To combine regions A, B, C, and D, equilibrium and compatibility conditions must be considered. The equilibrium condition for the axial force is

$$P_A + P_D = P_B + P_C = P_T \tag{A5}$$

Compatibility requires the shortening of regions A and D to be identical. Hence,

$$\alpha_A\,\Delta T a + \frac{P_A a}{S_A} = a - \bar{a} \tag{A6}$$

Equations (A3) through (A6) can be combined to obtain the governing equation for the laminate.

$$P_T = \frac{\pi^2 S_A}{a^2}\left[\frac{1}{16}\left(\delta^2 + 2\delta\delta_o\right) + \frac{D(S_A + S_D)}{S_A S_D}\frac{\delta}{\delta + \delta_o}\right] - (\alpha_A - \alpha_D)\,\Delta T S_A \qquad (A7)$$

For a specified load P_T, equation (A6) is solved using a Newton-Raphson technique to obtain δ. P_D can then be calculated using equation (A3). From static equilibrium, the moment acting on the delaminated region at the crack tip is

$$M = \frac{P_D}{2}(\delta + \delta_o) = \frac{\pi^2 D}{2a^2}\,\delta \qquad (A8)$$

The force P_C is found from rule of mixtures by solving equations (A9):

$$\begin{aligned} P_B + P_C &= P_T \\ P_B &= S_A(\varepsilon - \alpha_A\,\Delta T) \\ P_C &= S_D(\varepsilon - \alpha_D\,\Delta T) \end{aligned} \qquad (A9)$$

where ε is the axial strain in regions B and C. The result is

$$P_C = \frac{S_D}{S_A + S_D}\left[P_T - S_A\,\Delta T(\alpha_D - \alpha_A)\right] \qquad (A10)$$

APPENDIX B

CALCULATION OF CRITICAL LOADS

This appendix describes the procedures used to calculate critical loads for delamination growth based on the three criteria in equations (27) through (29). The procedure is different for each criterion, so they are discussed separately.

Criterion: $G_I = G_{Ic}$

By combining equations (5), (6), and (18), the mode I strain-energy release rate can be expressed as a function of δ.

$$G_I = C_1\left(A_1\delta^2 + A_2\delta\right)^2 \tag{B1}$$

where

$$C_1 = \frac{\pi^4}{8a^4 b\Delta a}\,\frac{d_{y1}}{F_{y1}}$$

$$A_1 = \frac{S_A S_D}{8(S_A + S_D)}\,F_{y1}$$

$$A_2 = 2A_1\delta_o + DF_{y2}$$

For $G_I = G_{Ic}$ equation (B1) can be explicitly solved for δ.

$$\delta = \frac{-A_2 \pm \sqrt{A_2^2 - 4A_1\sqrt{G_{Ic}/C_1}}}{2A_1} \tag{B2}$$

The critical lateral deflection is the smallest of the two values from equation (B2). The corresponding critical load is determined by using the critical δ in equation (2).

Criterion: $G_M = G_{Ic}$

By combining equations (5) and (15), the strain-energy release rate due to the moment can be expressed in terms of δ.

$$G_M = \frac{\pi^4 D}{8a^4 b}\,\delta^2 \tag{B3}$$

For $G_M = G_{Ic}$ equation (B3) can be explicitly solved for δ.

$$\delta = \frac{2a^2}{\pi^2}\sqrt{\frac{2b}{D}\,G_{Ic}}$$

The corresponding critical load is determined by using this critical δ in equation (2).

Criterion: $\left(\frac{G_I}{G_{Ic}}\right)^2 + \left(\frac{G_{II}}{G_{IIc}}\right)^2 = 1$

The first step is to express both G_I and G_{II} in terms of δ. The equation for G_I has already been derived - equation (B1). The expression for G_{II} is obtained in a similar manner and is given in equation (B4).

$$G_{II} = C_2\left(A_3\delta^2 + A_4\delta\right)^2 \tag{B4}$$

where

$$C_2 = \frac{\pi^4}{8a^4 b\Delta a}\,\frac{d_{x1}}{F_{x1}}$$

$$A_3 = \frac{S_A S_D}{8(S_A + S_D)}\,F_{x1}$$

$$A_4 = 2A_3\delta_o + DF_{x2}$$

Substitution of the expression for G_I (eq. (B1)) and G_{II} (eq. (B2)) into the failure criterion yields a nonlinear equation in terms of δ.

This nonlinear equation was solved using the Newton-Raphson method. An initial guess of $\delta = 0.3$ mm was used for much of the calculations. However, the stability of the iterative solution did not appear to be very sensitive to the initial guess for δ. Once δ was determined, the critical load was calculated using equation (2).

TABLE 1.- LAMINATE PROPERTIES AND UNIT LOAD SOLUTIONS FOR SEVERAL LAMINATE TYPES

(b = 25.4 mm, Δa = .0254 mm)

	Laminate type†			
	1*	2	3	4
S_A, N	14.59E6	13.45E6	13.45E6	13.78E6
S_D, N	1.475E6	1.967E6	1.087E6	2.950E6
D, $N \cdot m^2$	.02159	.05118	.04546	.1727
F_{x1}	.0936	.0827	.108	.0689
F_{x2}, m^{-1}	531.	345.	366.	188.
F_{y1}	.0261	.0231	.0301	.0192
F_{y2}, m^{-1}	-252.	-164.	-174.	-89.1
d_{x1}, $m \cdot N^{-1}$	1.40×10^{-10}	1.24×10^{-10}	1.62×10^{-10}	1.03×10^{-10}
d_{y1}, $m \cdot N^{-1}$	2.97×10^{-10}	2.62×10^{-10}	3.43×10^{-10}	2.18×10^{-10}

*Unit load solutions for laminate type 1 are from reference 8. Solutions for other laminates were obtained using the technique described in the text.

†

Laminate type	Laminate
1	$[0_3/\overset{\downarrow}{0}/(0/45/90/-45)_{7s}/0_4]$
2	$[0_4/\overset{\downarrow}{(0/45/90/-45)_{7s}}/0/45_2/0]$
3	$[0/90_2/\overset{\downarrow}{0}/(0/45/90/-45)_{7s}/0/45_2/0]$
4	$[0_6/\overset{\downarrow}{0_2}(0/45/90/-45)_{6s}/0_3/45/90_2/45/0]$
The delamination location is indicated by the arrow.	

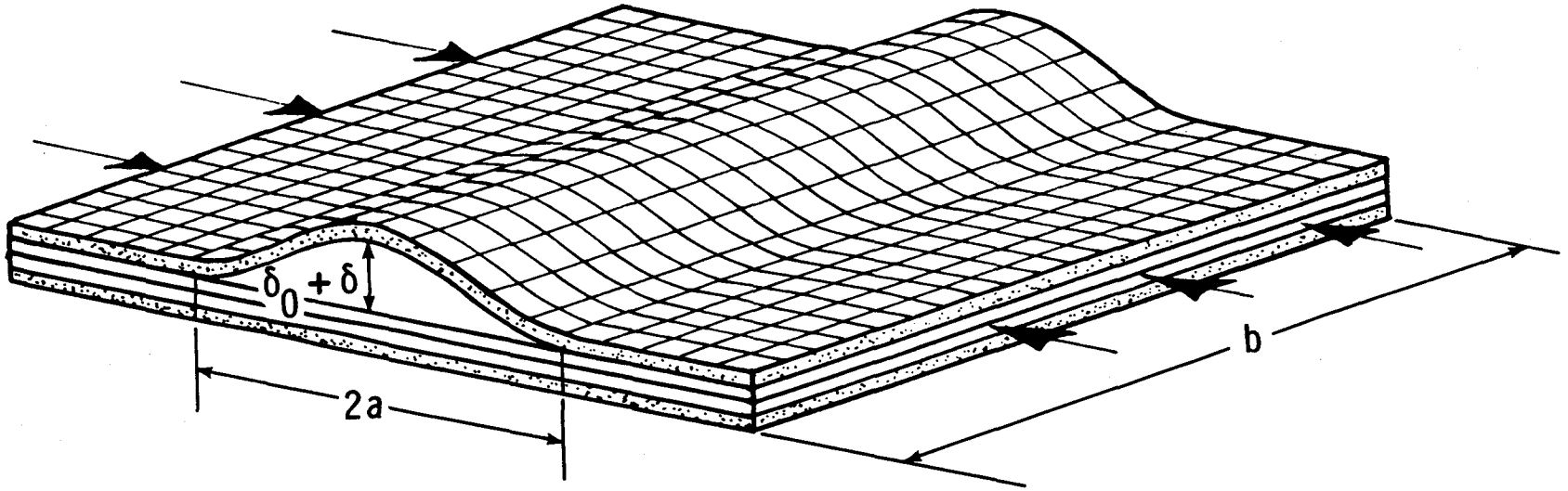

Figure 1. - Local buckling of laminate with through-width delamination.
(δ_0 = initial imperfection)

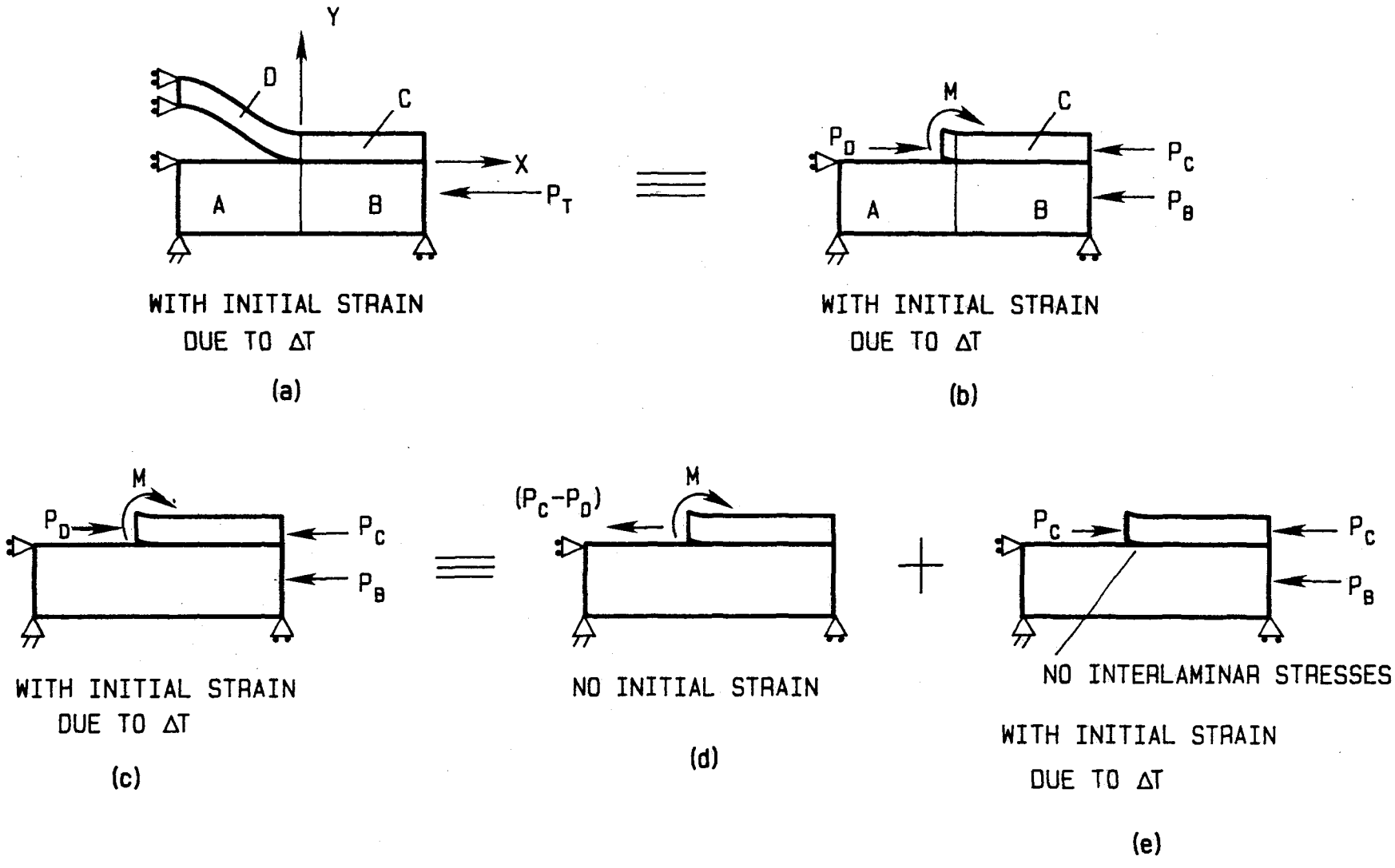

Figure 2. - Nonlinear configuration (a) transformed into linear configuration (d) with two nonlinearly related loads, $(P_C - P_D)$ and M.

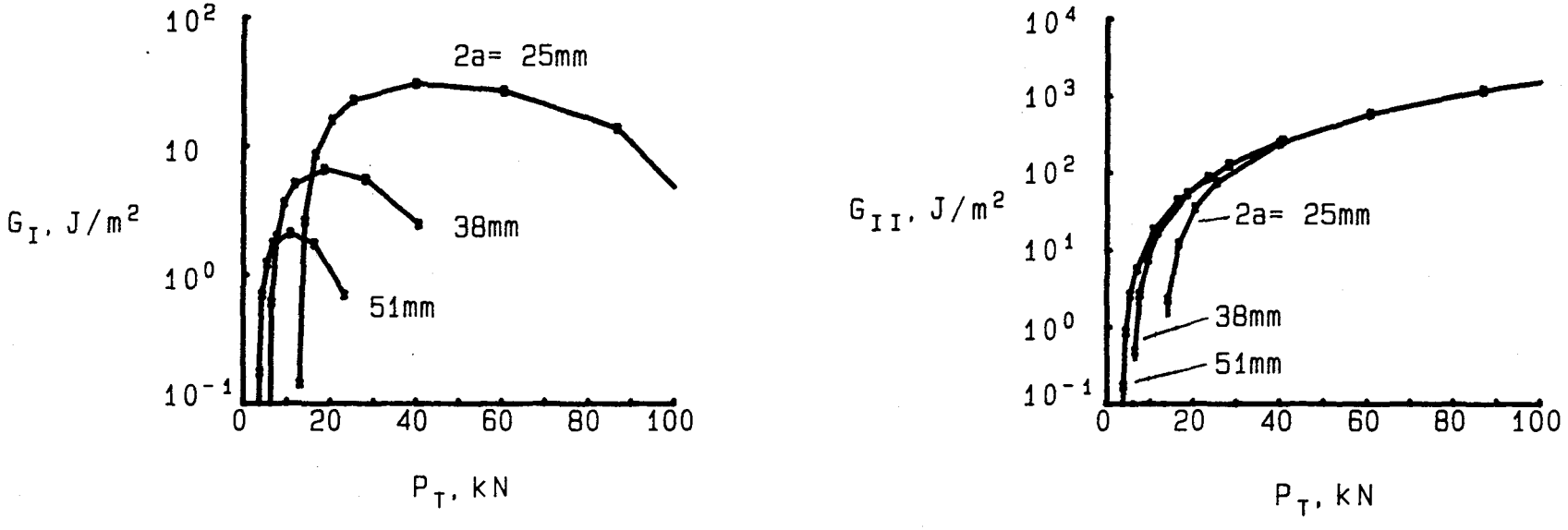

(a) Effect of delamination length for laminate type 1

Figure 3. - Effect of various parameters on G_I and G_{II} vs. applied load.
(Initial imperfection $\delta_o = 0$)

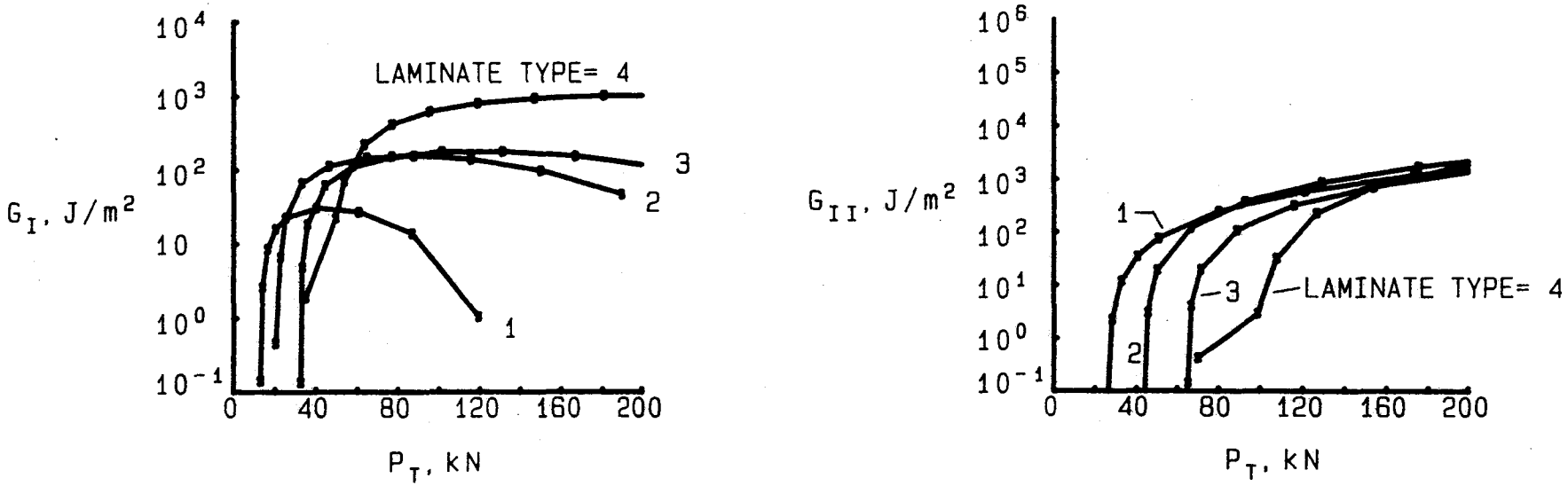

(b) Effect of laminate type
(Delamination length = 25 mm)

Figure 3. - Concluded.

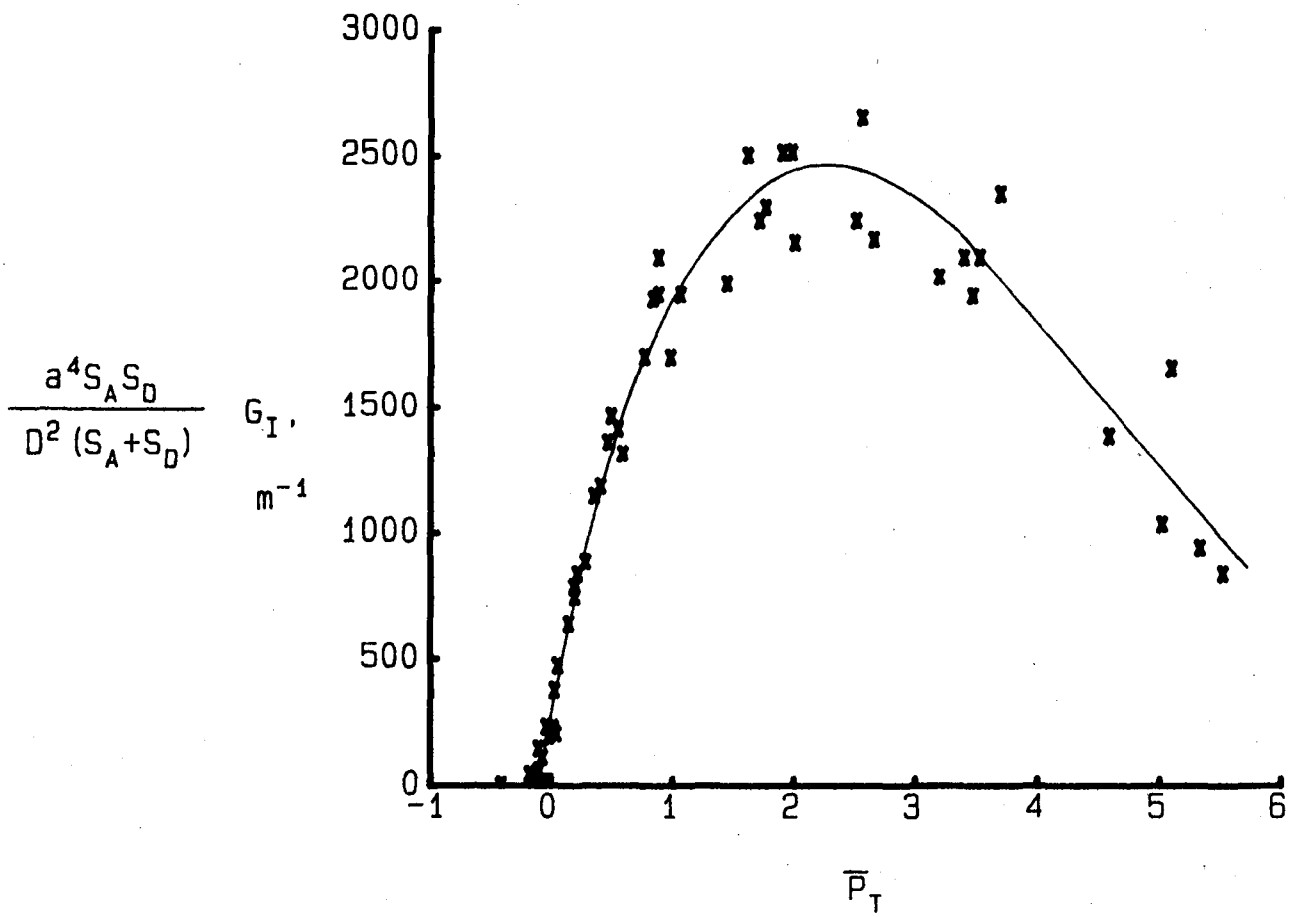

(a) Normalized G_I vs. normalized load

Figure 4. - Normalized plots of G_I and G_{II} vs. applied load. These plots include all of the data in Figure 3. (Curves are visual fit of data.)

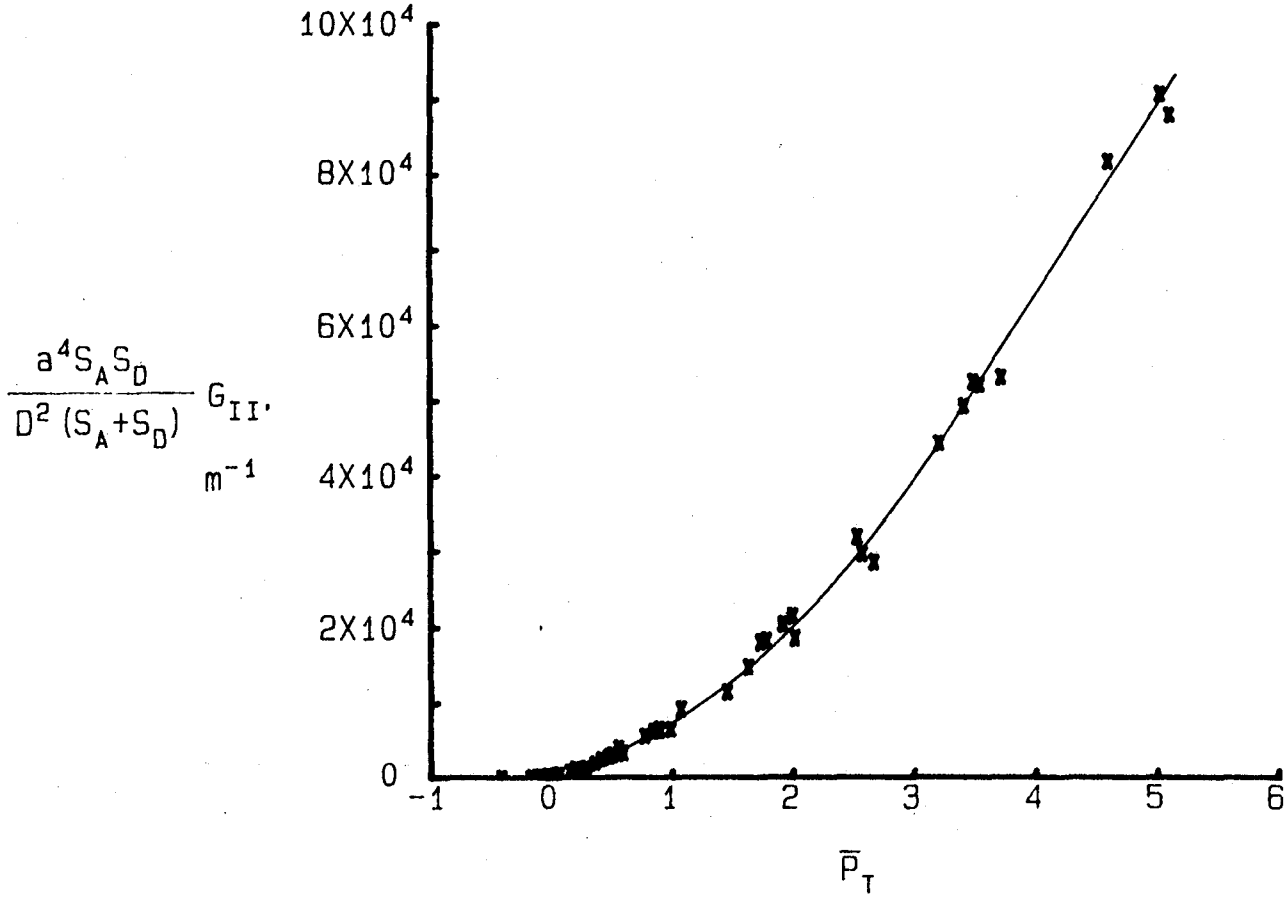

(b) Normalized G_{II} vs. normalized load

Figure 4. - Concluded.

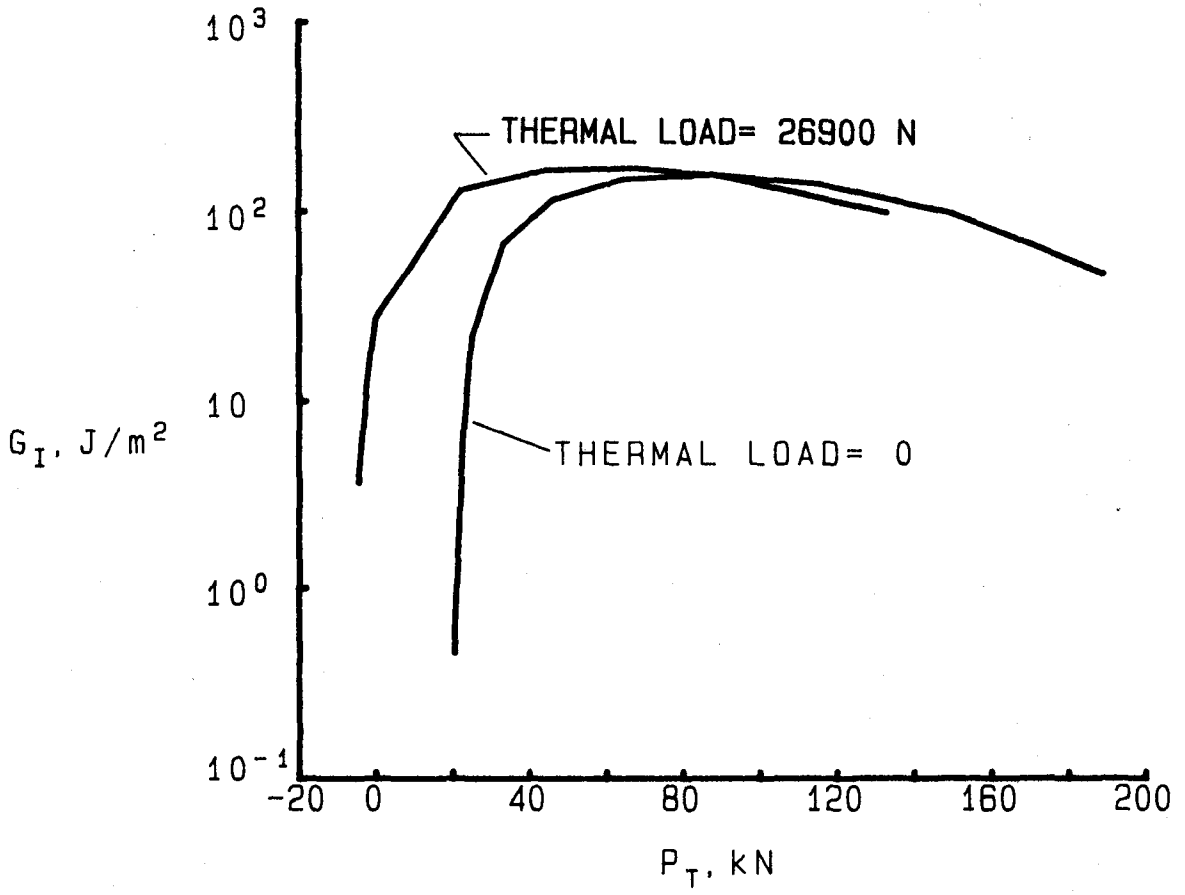

(a) G_I vs. applied load.

Figure 5. - Effect of thermal load on G_I vs. applied load. The thermal load is due to an initial strain $(\alpha_A - \alpha_D)\Delta T = .002$. (delamination length = 25 mm, initial imperfection, $\delta_o = 0$; laminate type 2)

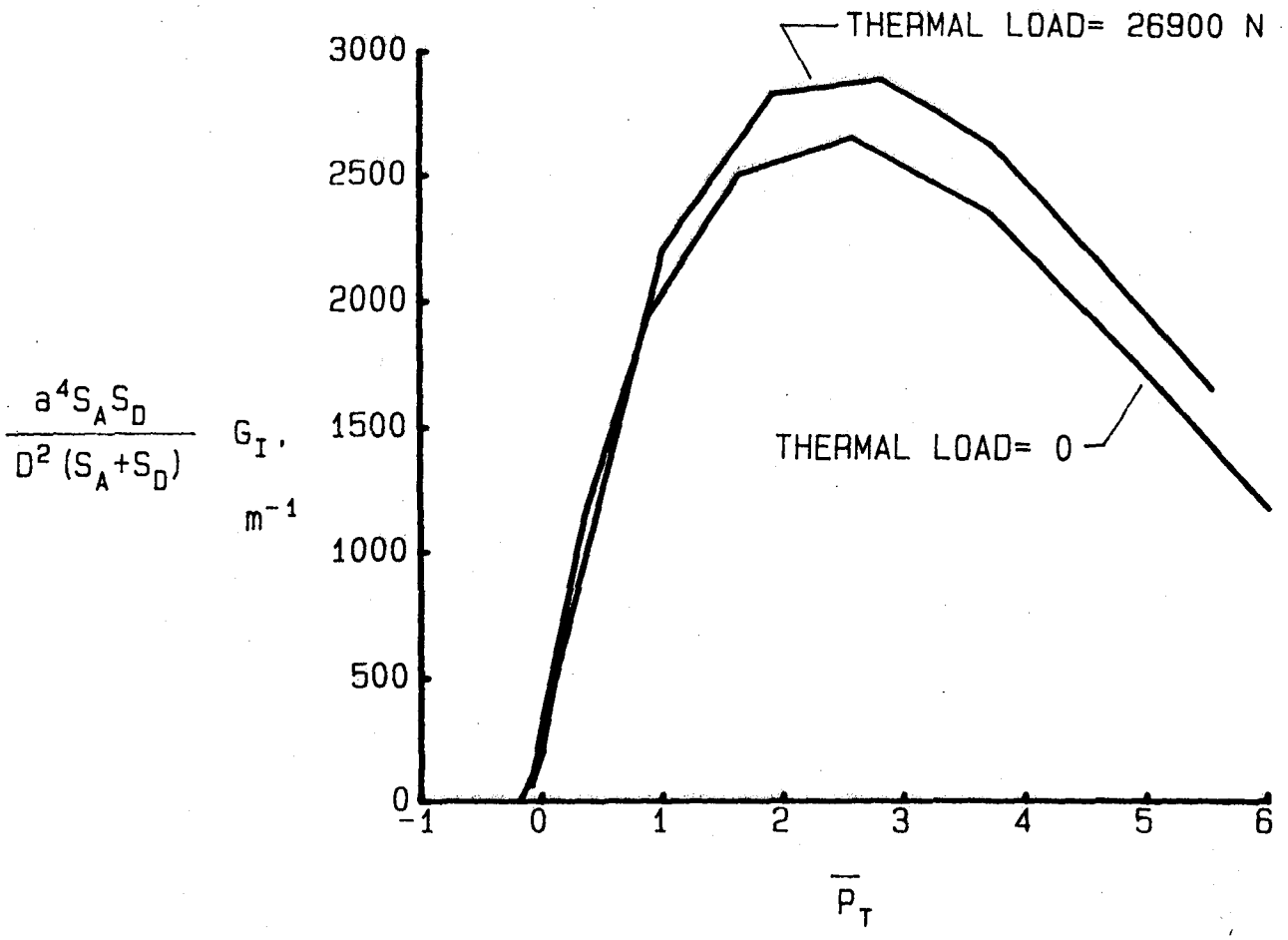

(b) Normalized G_I vs. normalized load

Figure 5. - Concluded.

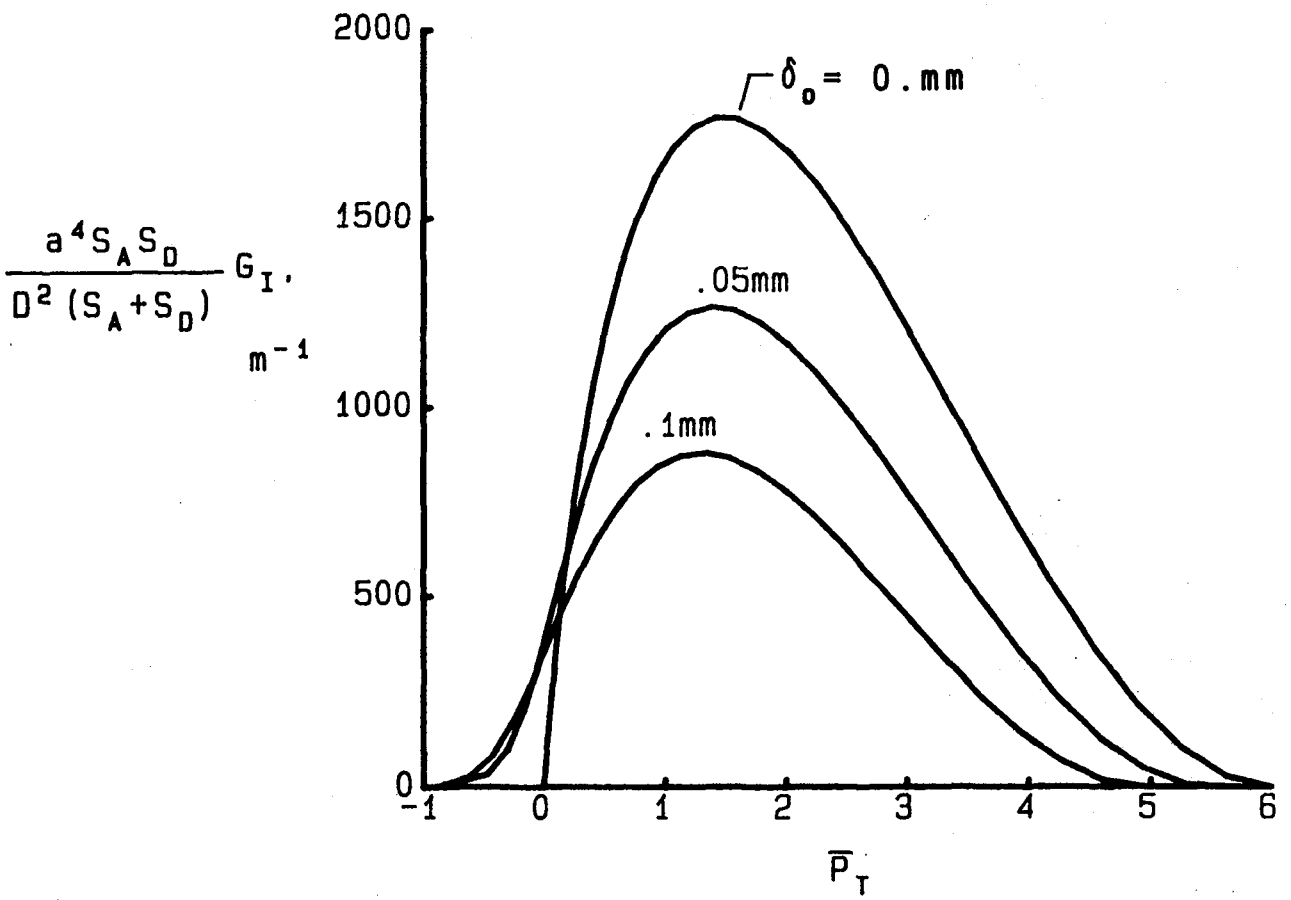

(a) Effect on normalized G_I

Figure 6. - Effect of initial imperfection on normalized G_I and G_{II} vs. applied load. (laminate type = 1; arbitrary delamination length)

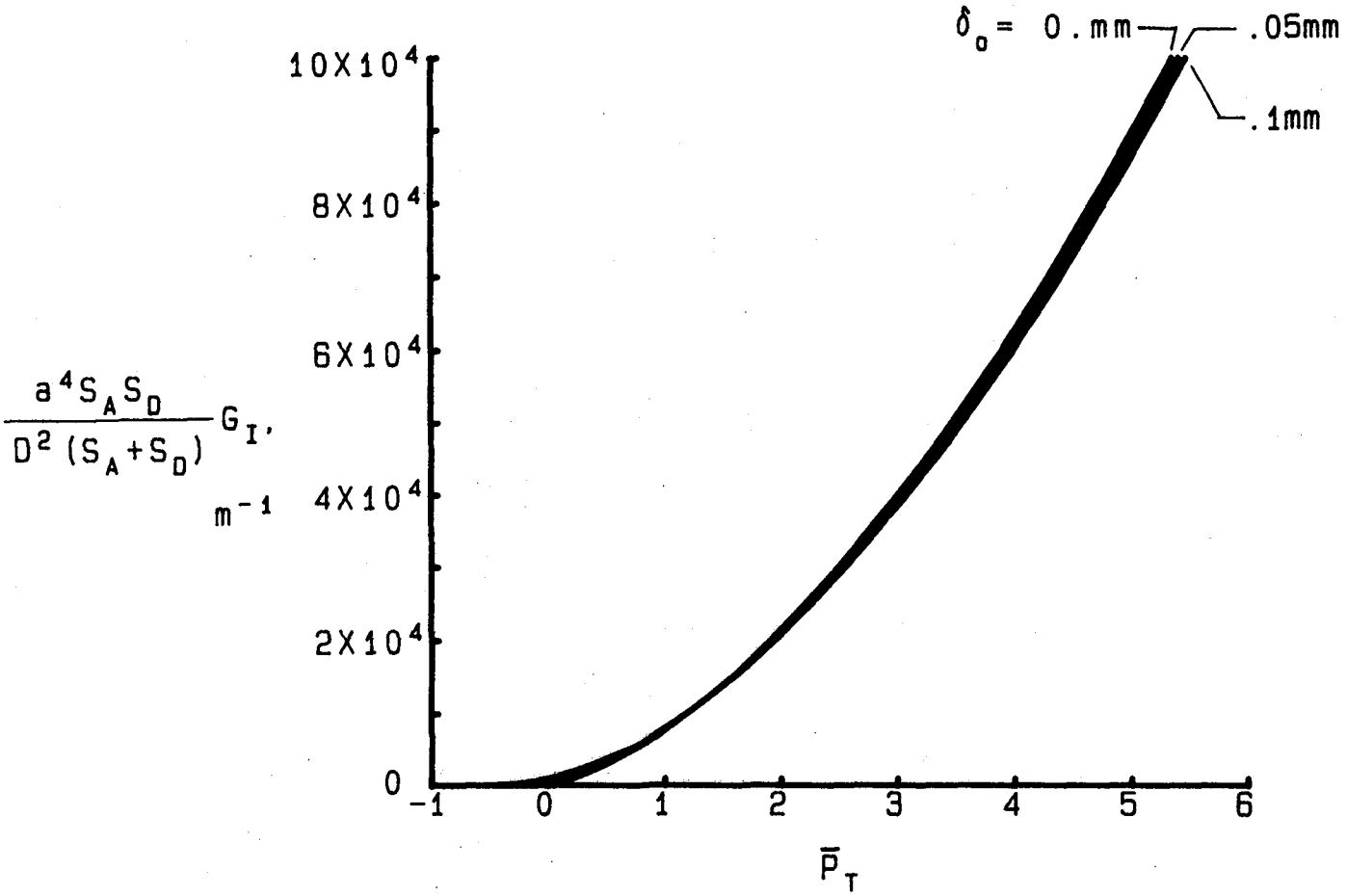

(b) Effect on normalized G_{II}

Figure 6. - Concluded.

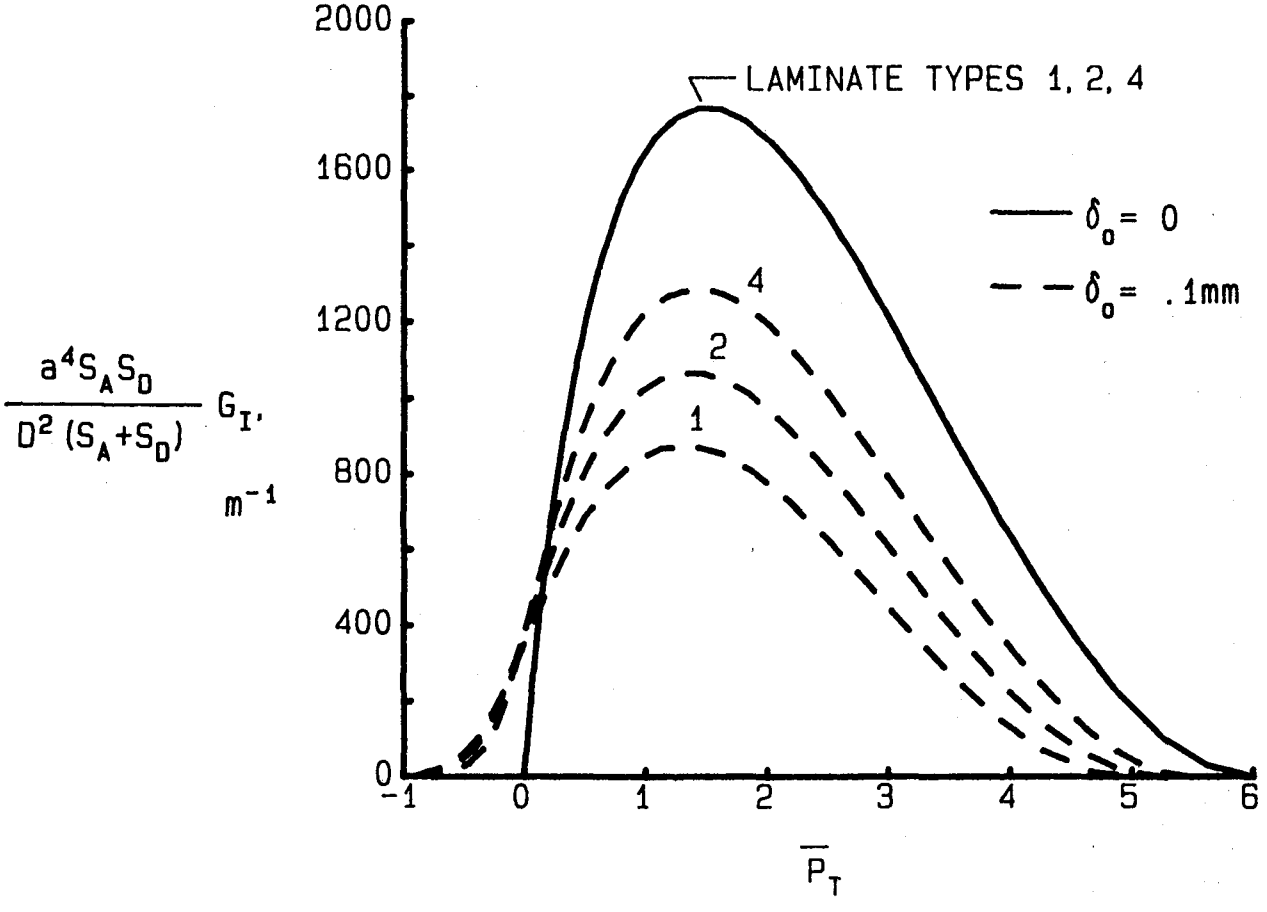

(a) Effect on normalized G_I

Figure 7. - Effect of laminate type and initial imperfection on normalized G_I and G_{II}. (arbitrary delamination length)

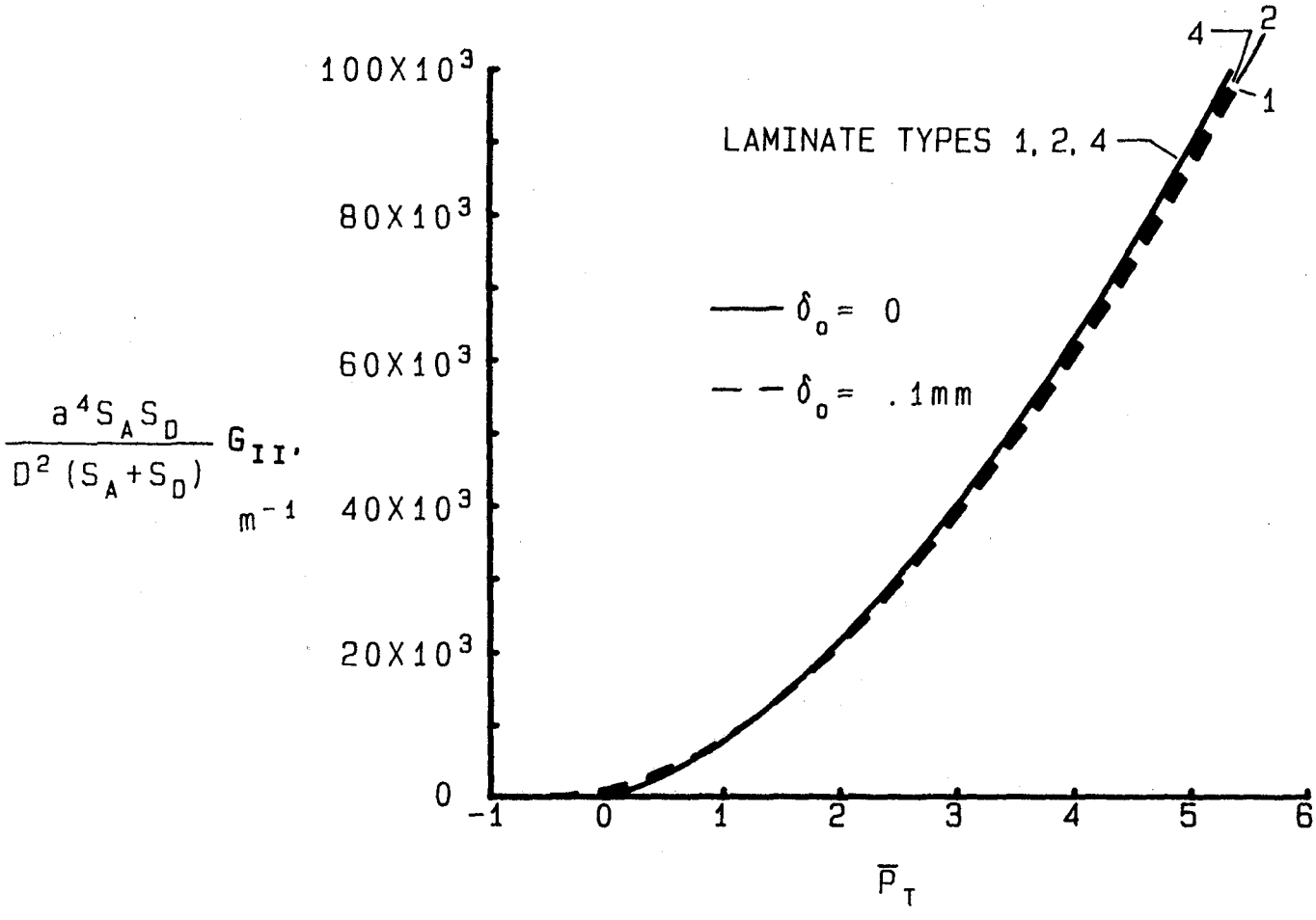

(b) Effect on normalized G_{II}

Figure 7. - Concluded.

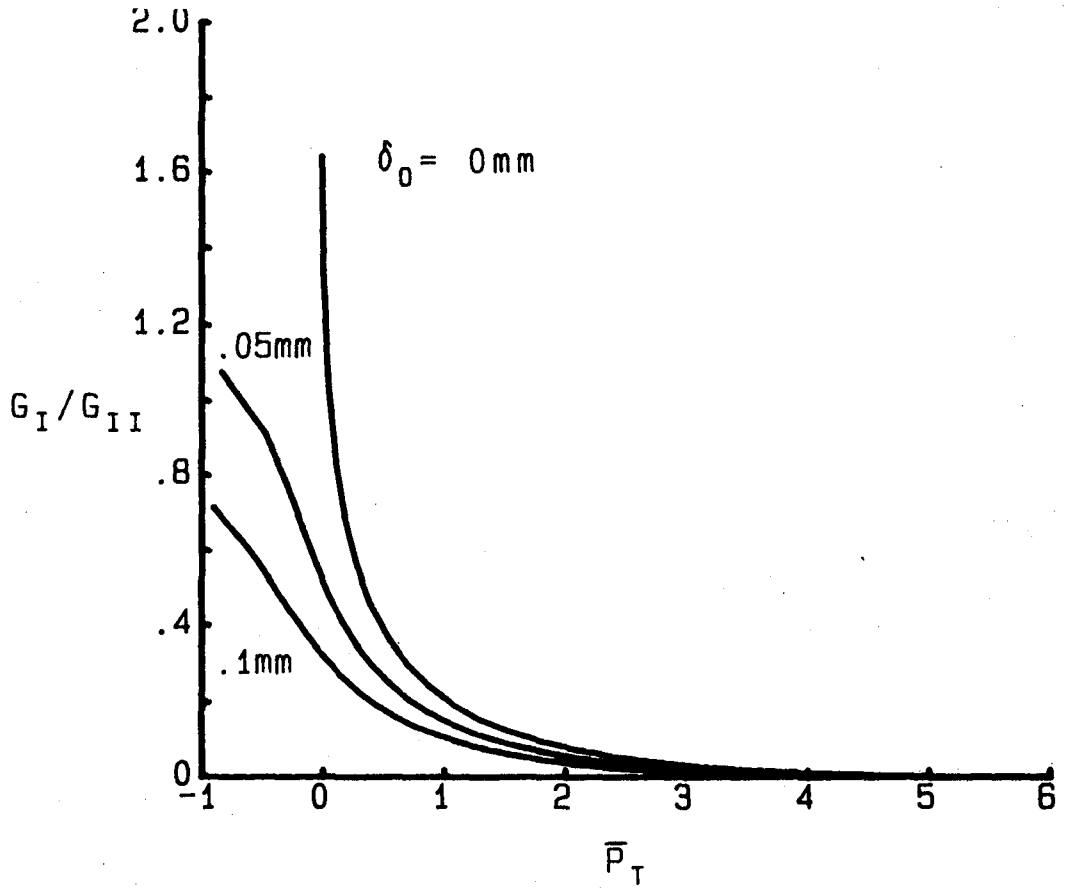

Figure 8. - Effect of initial imperfection on G_I/G_{II} vs. normalized applied load. (laminate type = 1; arbitrary delamination length)

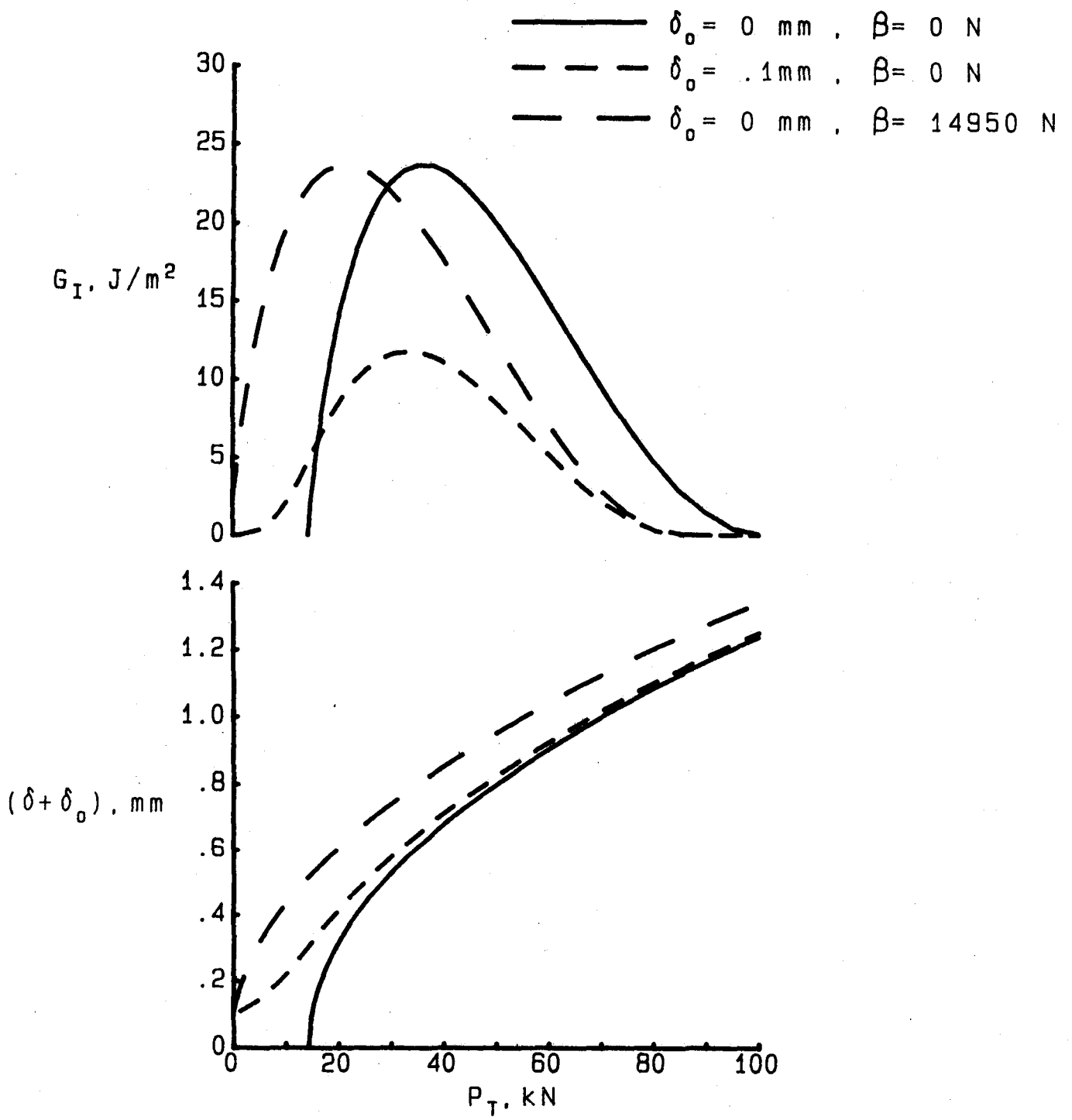

Figure 9. - Comparison of G_I and total deflection $(\delta + \delta_0)$ vs. applied load for three cases of initial imperfection δ_0 and thermal load β. (laminate type = 1)

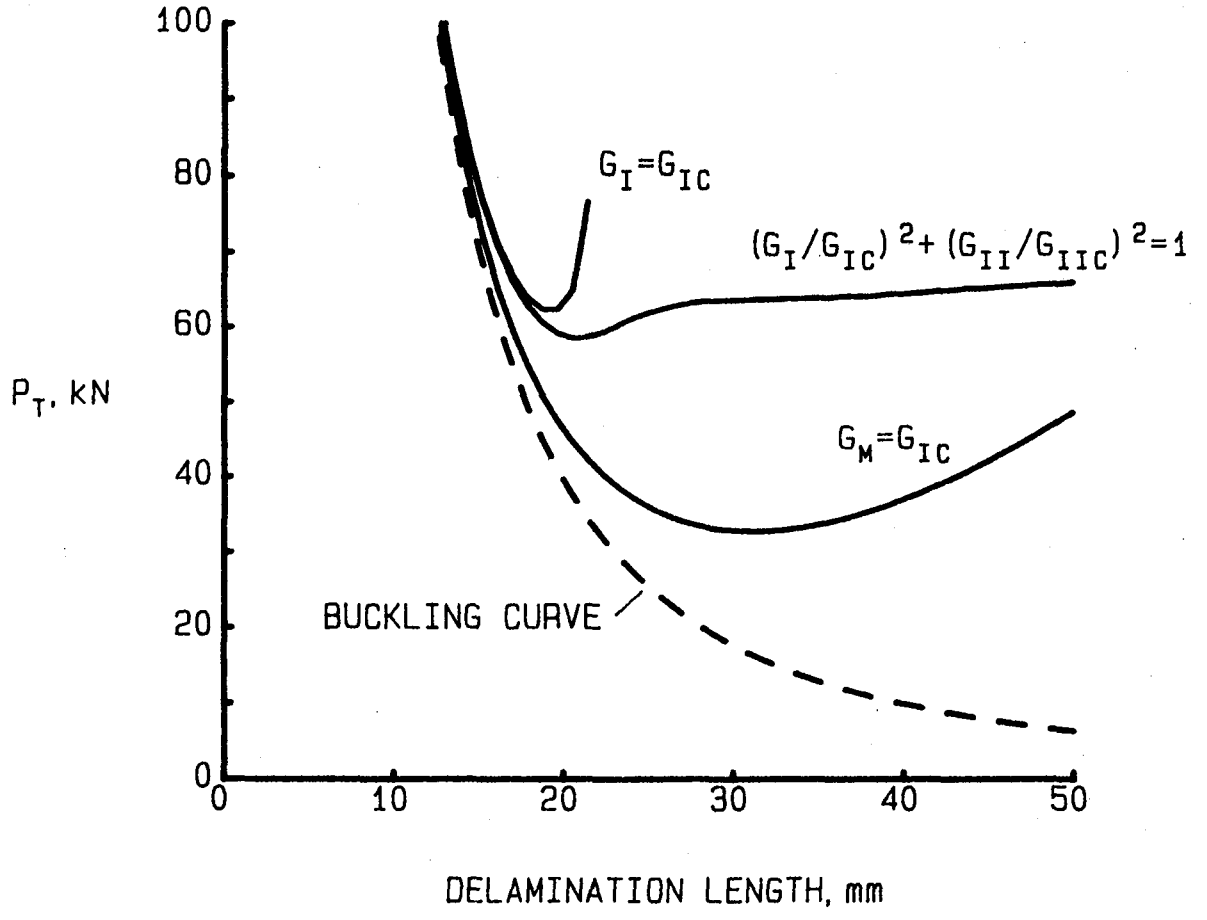

Figure 10. - Critical load for delamination growth using three growth criteria. Buckling curve shown for reference. (G_{Ic} = 200 J/m^2; G_{IIc} = 1000 J/m^2; laminate type = 2; initial imperfection δ_o = 0).

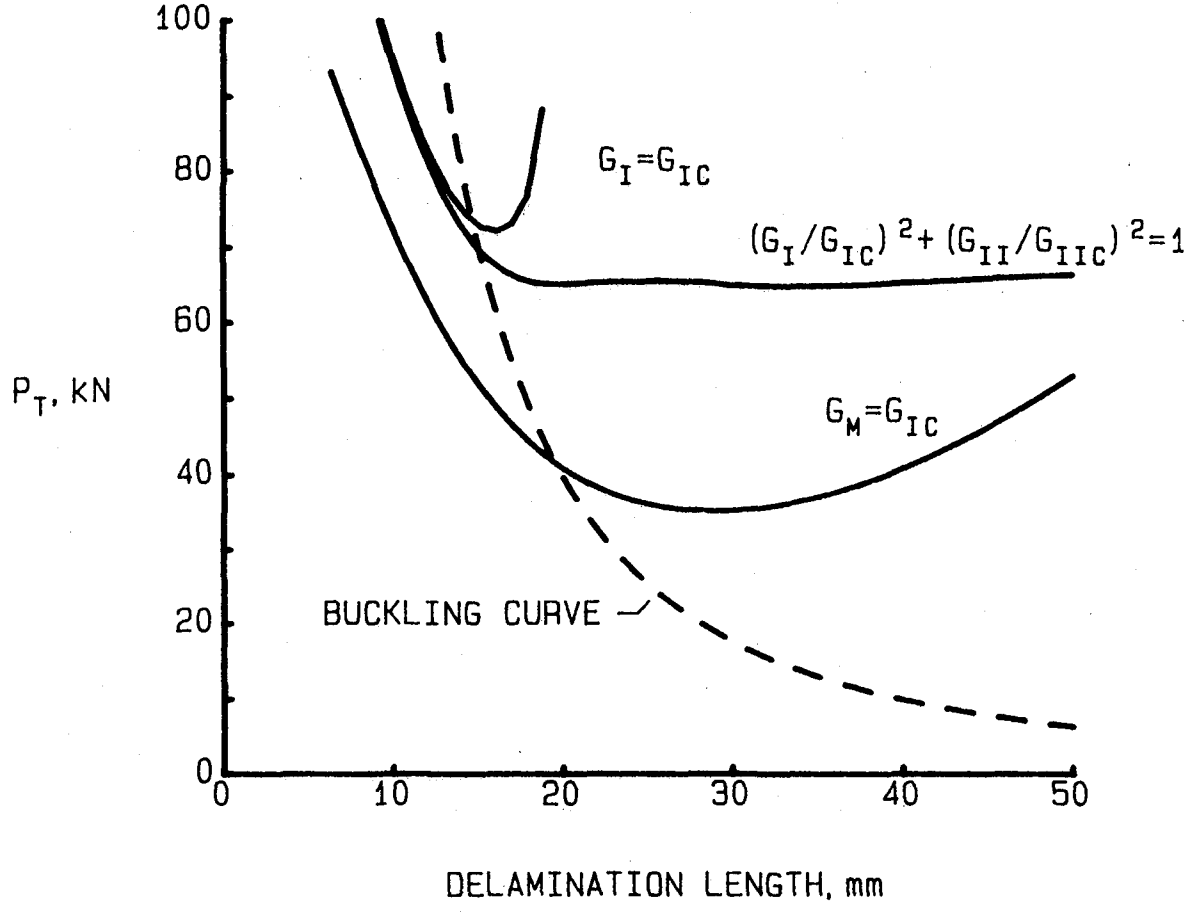

Figure 11. - Critical load for delamination growth using three growth criteria. Buckling curve shown for reference. (G_{Ic} = 200 J/m^2; G_{IIc} = 1000 J/m^2; laminate type = 2; initial imperfection δ_o = .1mm).

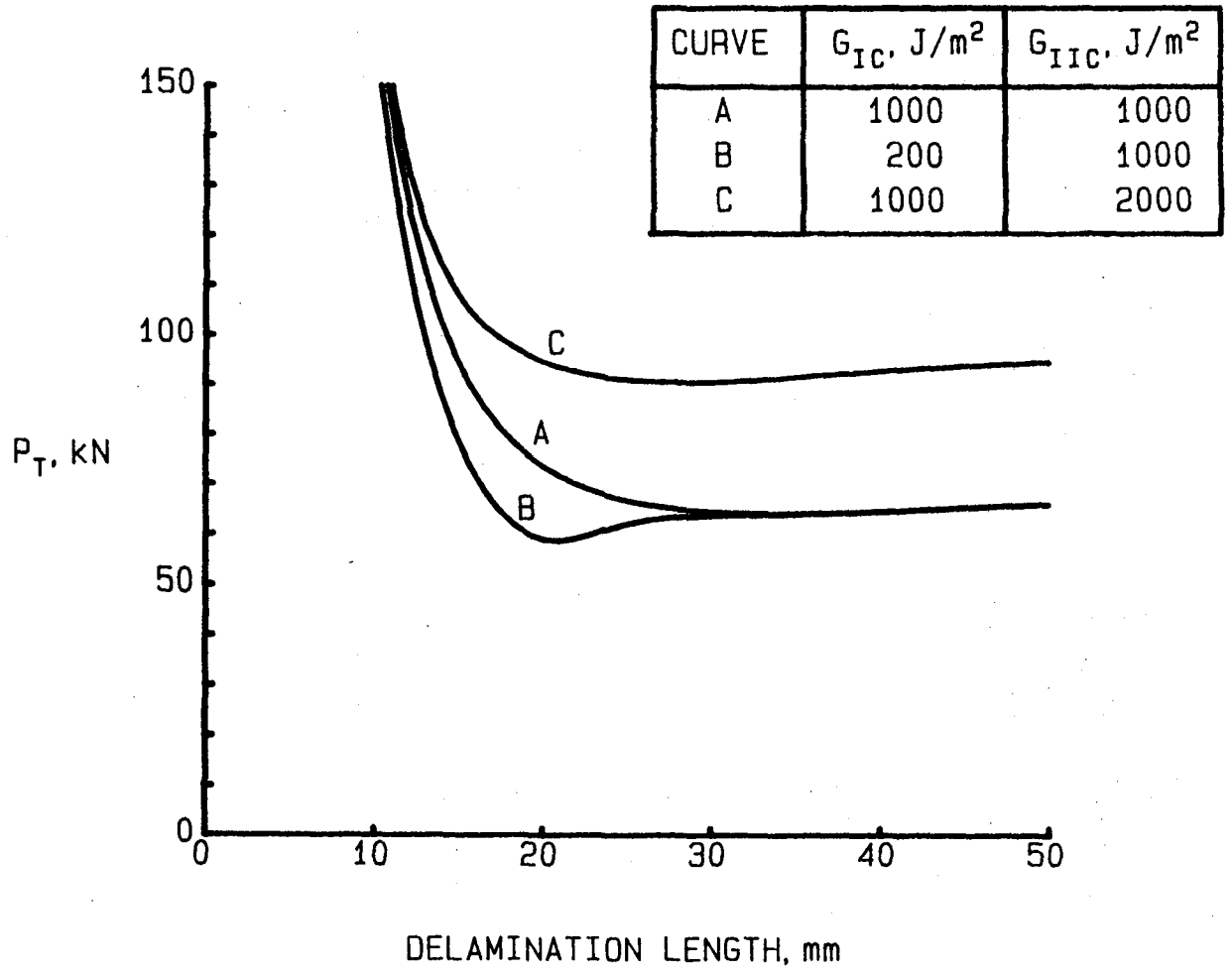

Figure 12. - Effect of G_{Ic} and G_{IIc} on critical load predicted by mixed mode criterion. (laminate type = 2; initial imperfection $\delta_o = 0$)

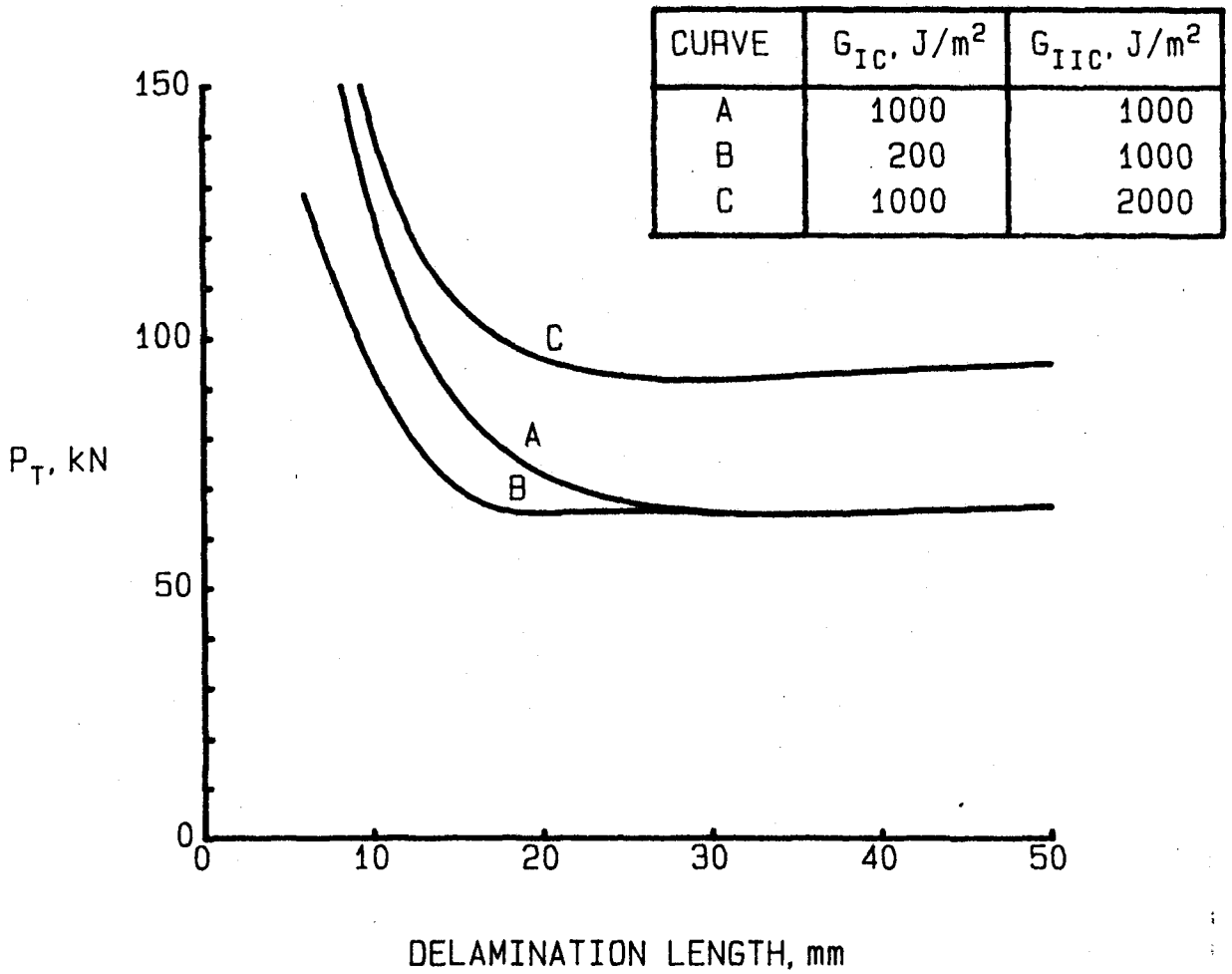

Figure 13. - Effect of G_{Ic} and G_{IIc} on critical load predicted by mixed-mode criterion. (laminate type = 2; initial imperfection δ_o = .1mm).

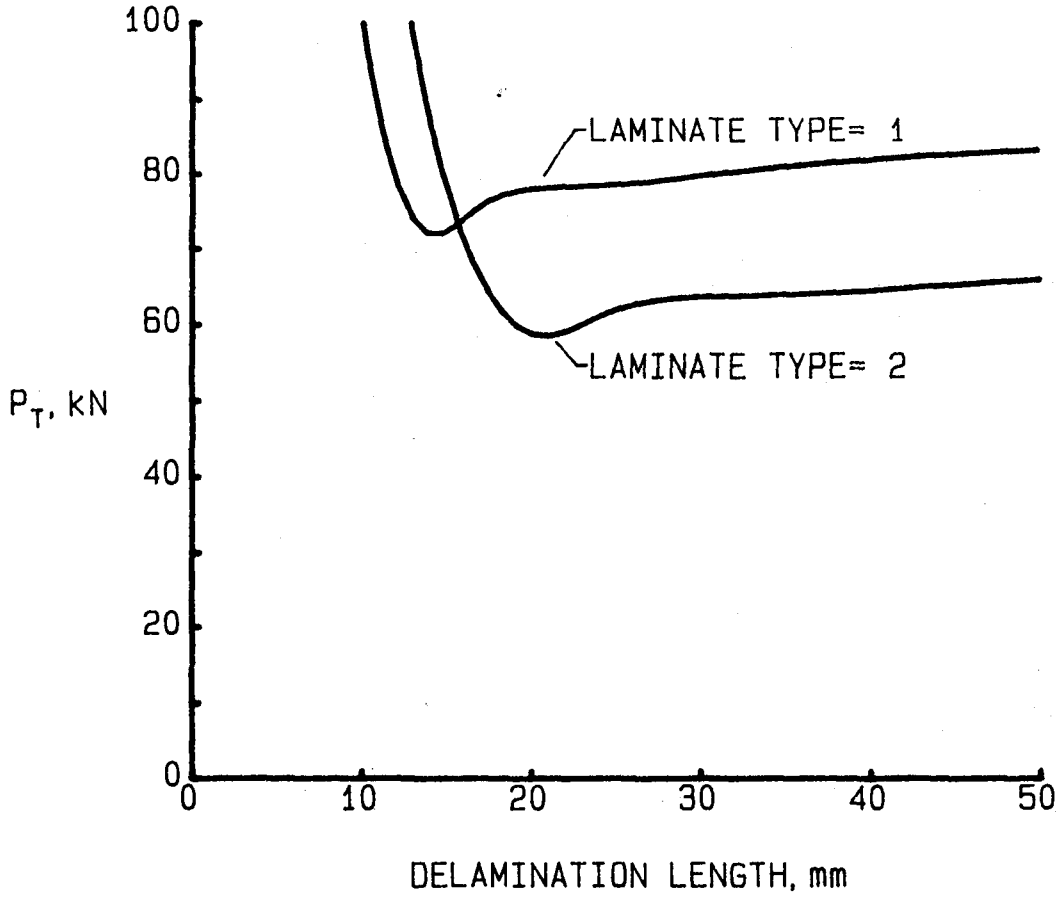

Figure 14. - Effect of laminate type on critical load predicted by mixed-mode criterion. (G_{Ic} = 200 J/m^2; G_{IIc} = 1000 J/m^2; initial imperfection δ_0 = 0).

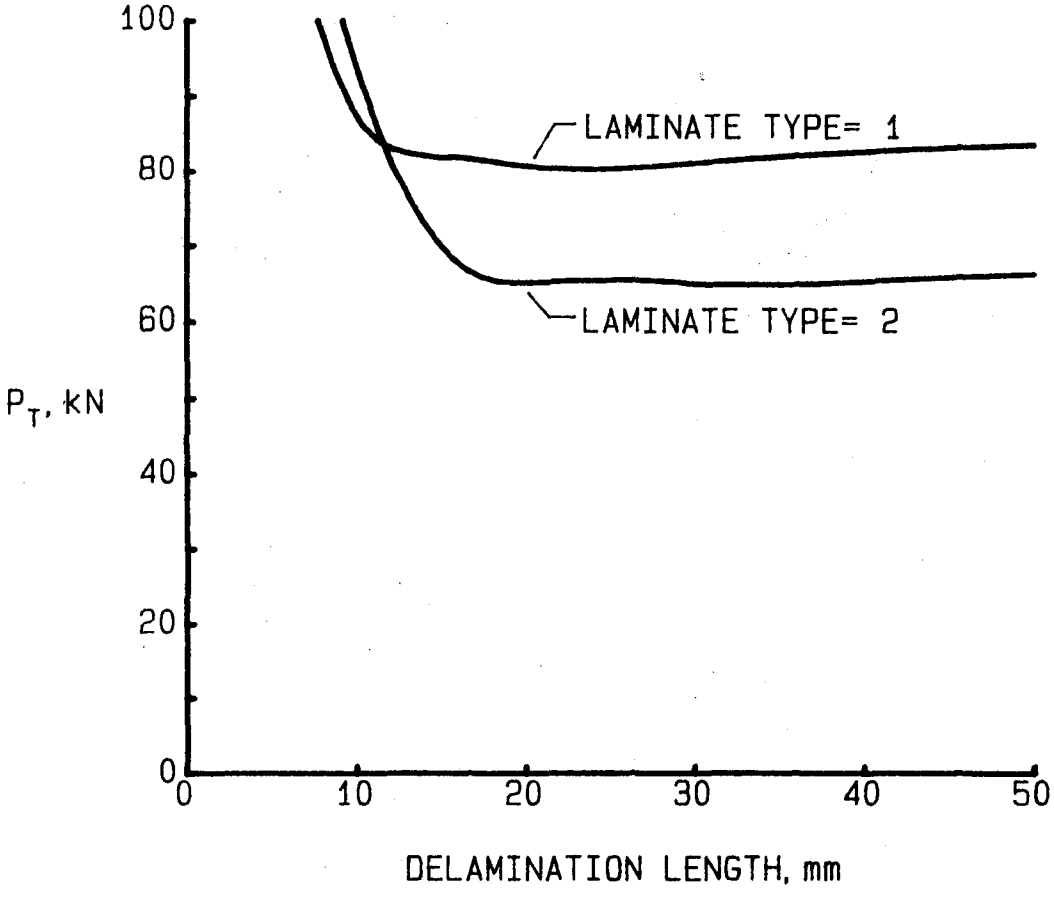

Figure 15. - Effect of laminate type on critical load predicted by mixed-mode criterion. (G_{Ic} = 200 J/m^2; G_{IIc} = 1000 J/m^2; initial imperfection. δ_o = .1mm).

1. Report No.	2. Government Accession No.	3. Recipient's Catalog No.
NASA TM-86301		

4. Title and Subtitle	5. Report Date
Analysis of Instability-Related Growth of a Through-Width Delamination	September 1984
	6. Performing Organization Code: 534-06-23-03

7. Author(s)	8. Performing Organization Report No.
John D. Whitcomb	
	10. Work Unit No.
9. Performing Organization Name and Address: NASA Langley Research Center, Hampton, VA 23665	11. Contract or Grant No.
	13. Type of Report and Period Covered: Technical Memorandum
12. Sponsoring Agency Name and Address: National Aeronautics and Space Administration, Washington, DC 20546	14. Sponsoring Agency Code

15. Supplementary Notes

16. Abstract

When a laminated composite is subjected to compressive loads, a delaminated region may buckle. This causes high interlaminar stresses at the delamination front and the delamination may grow. The effect of various parameters on instability-related delamination growth was studied analytically. The configuration studied consisted of a thick composite laminate with a single through-width delamination located near one surface. Both mechanical and thermal loads were considered. All conclusions were based on the assumption that G_I and G_{II} govern delamination growth. An approximate superposition stress analysis was developed which gives closed form expressions for G_I and G_{II}. The simplicity of the analysis permitted examination of numerous configurations. Both G_I and G_{II} were found to be very sensitive to delamination length and location through the thickness. The magnitude of G_I was also very sensitive to initial imperfection. Critical loads for delamination growth were calculated based on three growth criteria. Large differences in the predictions highlight the need for a verified mixed-mode delamination growth criterion.

17. Key Words (Suggested by Author(s))	18. Distribution Statement
composite materials, laminates, delamination, local buckling, nonlinear stress analysis, compression	Unclassified - Unlimited Subject Category - 24

19. Security Classif. (of this report)	20. Security Classif. (of this page)	21. No. of Pages	22. Price
Unclassified	Unclassified	56	A04

For sale by the National Technical Information Service, Springfield, Virginia 22161